COO-2249-3

Department of Meteorology, 54-1517

Massachusetts Institute of Technology

Cambridge, Massachusetts 02139

Transport Processes and Trace Constituents in the Stratosphere

Annual Progress Report

Research conducted under Contract no. AT(11-1)-2249

Principal Investigator: Dr. Derek M. Cunnold

Mar. 15, 1974

DISCLAIMER

Table of Contents

Excellent progress has been made under contract number AT 11-1-2249 during the past year particularly in the modeling activities of task I. The progress in each of the research areas is outlined under the individual task headings.

(I) Numerical modeling

The modeling activities of task I have attained a significant milestone with the accomplishment of two 3 year integrations of the model. Both integrations were for conditions believed to exist in the unperturbed stratosphere. The results of the first run were presented at the IAMAP/IAPSO International Conference on the Structure, Composition, and General Circulation of the Upper and Lower Atmospheres and Possible Anthropogenic Perturbations held on January 14-25, 1974 in Melbourne, Australia. The results of the second integration, in which a few minor adjustments were made to correct some minor deficiencies of the first integration, were presented at the Third Conference on the Climatic Impact Assessment Program held in Cambridge, Mass. on Feb. 26-Mar. 1, 1974. A copy of this paper is enclosed as attachment A. This second integration produced slightly better agreeement between the model results and the atmospheric observations. In both runs moreover the model reproduced many of the observed dynamical features of the stratosphere and of the observed global stratospheric ozone distribution.

The model gives a westerly wind maximum in the stratosphere of the observed amplitude and location in winter which changes

over to easterlies in summer. Furthermore, the lower stratosphere is being forced by the troposphere while the troposphere and the upper stratosphere are largely forced by the in-situ distribution of heating and cooling. The model shows ozone to be transported polewards and downwards and the poleward eddy flux is of the same magnitude as is observed. Moreover, the general level of fluctuations of columnar ozone are correctly predicted as is the seasonal variation in ozone at mid-latitudes. The standing wave patterns of columnar ozone also seem to agree well with the observations. The only significant deficiency in the model is that the pole to equator gradients of ozone are not as large as those observed particularly during the winter and the spring. An attempt is underway to remove this deficiency by adding a realistic latitudinal distribution of NO_2 and by reducing the diffusion coefficient (perhaps to zero) everywhere except in the atmospheric boundary layer.

The remote terminal to the IBM 360/95 at Goddard Institute for Space Studies has worked well over the past year and machine time has been available to us at a fairly satisfactory level.

(II) Stratospheric data analysis

5 years of daily values of Z and T at levels between 200 and 10 mb and for latitudes between 20°N and the pole have been used to derive geostrophic winds in the stratosphere. The data has been analysed to produce monthly statistics on the wind and temperature fields in the stratosphere. Some of the results

were presented in a Frontiers talk entitled "The general circulation, thermal structure, and energetics of the stratosphere" by Prof. R.E. Newell, G. Herman, J. Fullmer, and M. Tanaka and presented at the IAMAP/IAPSO Conference in Melbourne. This paper is being published as an M.I.T. Department of Meteorology Report, copies of which will be submitted to the AEC shortly.

For comparison with the results of the numerical model the contribution of each planetary wave to the covariances of meridional velocity and temperature and the correlation between meridional velocity and temperature at mid-latitudes have been calculated. A preliminary comparison between this data and the model results has been made. At the present time we are somewhat concerned with the adequacy of the observational data particularly at the higher planetary wavenumbers. We plan to look into this question and to make additional comparisons between the observational results and the model predictions during the next year.

(III) Effect of trace constituents on heating rates

The contribution of particulates resulting from SST operations to heating in the stratosphere has been calculated and found to be considerably smaller than the heating due to the ambient gases of the stratosphere. This work is described in attachment B. Because the heating rate due to SST aerosols appears to be so small it has been decided that the construction

of an aerosol coagulation code would constitute an unnecessary degree of sophistication for computing the aerosol heating. Because the results of the general circulation model appear to simulate the stratosphere remarkably well, there has been little incentive for us to test the range of validity of our parameterization of heating rates. We regard this as a low priority research item and will investigate this question as time permits.

In order to obtain a better understanding of the contribution of aerosols to heating in the present day stratosphere an attempt is being made to experimentally define the spatial and temporal variations of the natural aerosol physical properties through an analysis of "SKYLAB-EARTH RESOURCES EXPERIMENT PACKAGE" data. Utilizing the scattered sunlight horizon inversion technique developed for determining aerosol physical properties (Gray et al, 1973) the "SKYLAB-EREP" experimental data from EPN-587 is being analysed. The anticipated results will give vertical distributions of aerosol number density, size distribution and the real and imaginary components of the index of refraction in the altitude region of 10 to 100 km.

Data tapes and documentation are presently being received from the SKYLAB (SL3) mission with the initial steps of processing having begun. During the (SL-3) mission two horizon profile scans were obtained in the experimental mode (EPN-587) utilizing the Infrared Spectrometer (S-191). The first set of horizon

scans was on August 11, 1973 over the South Atlantic Ocean and the second set was on September 17, 1973 in a scan from Alaska to Cuba.

For the (SL-4) mission additional horizon profile data was gathered on December 5, 1973. On December 14, 1973 six sets of horizon profiles were obtained from New Zealand to Central America and on January 8, 1974 six horizon sets were obtained from Montana to Greenland. Other horizon scans are planned in the equatorial region during the remainder of this final mission and will be processed along with the present data to give a comprehensive evaluation of aerosol physical property distributions.

Personnel

The principal investigator has been employed full time on this contract during the current contract period. In January he presented a paper describing the results of the model at the IAMAP/IAPSO International Conference on the Structure, Composition, and General Circulation of the Upper and Lower Atmospheres and Possible Anthropogenic Perturbations in Melbourne, Australia. This project also contributed per diem expenses for G. Herman to attend the same conference and to present some results on the energetics of the natural stratosphere. Fred Alyea presented a paper describing the model at the Second Numerical Prediction Conference in Monterey in October. He decided however, not to attend the Numerical Simulation Conference in Novosibirsk. Most members of the project attend the Third Conference on the

Climatic Impact Assessment Program last month in Cambridge, Mass., where a paper was presented by D.M. Cunnold. Both Fred Alyea and D. Cunnold plan to attend the A.G.U. meeting in Washington, D.C. in April and to give a presentation there. They also visited Goddard Institute for Space Studies in New York in September in order to use the computer there.

Preliminary Results of the M.I.T. Photochemical-Dynamical Ozone Model

by

D.M .Cunnold, F.N. Alyea, N.A. Phillips and R.G . Prinn

Department of Meteorology

Massachusetts Institute of Technology

Cambridge, Massachusetts 02139

This paper was presented at the Third Conference on the Climatic Impact Assessment Program, Cambridge, Mass., Feb. 26 - Mar. 1, 1974

Abstract

This paper reports on a general circulation model being developed with the ultimate objective of assessing the effect of SST operations on the atmospheric ozone distribution. The model variables are represented in the spectral domain using 79 spherical harmonics and 26 vertical levels between the ground and 70 km. The results of a three year integration (run 12) to simulate the unperturbed global ozone distribution are presented in this paper. The model shows the presence of a westerly stratospheric jet in the winter hemisphere with amplitude similar to those observed in the polar night jet; easterlies dominate in the summer hemisphere. The model also shows ozone to be transported polewards and downwards. Furthermore the annual cycle in ozone concentrations at mid-latitudes has been simulated. Preliminary comparisons are also made with other features of the dynamics and ozone distribution in the stratosphere.

Introduction

This paper reports on a combined photochemical-dynamical (3-dimensional) model of the stratosphere which has been developed with the aim of simulating the observed global ozone distribution and of predicting the changes in that distribution resulting from the NO_x introduced by a fleet of supersonic transports (SST). In this paper model calculations on the dynamics of the unperturbed stratosphere and on the ozone distribution therein are presented. Two 3 year integrations have so far been performed. The first integration was reported on at the Melbourne IAMAP meeting (Cunnold et al, 1974). This paper contains the results of the second 3 year integration in which a few minor adjustments were made resulting in slightly better agreement between the calculated results and the observations of the natural stratosphere.

Stratospheric ozone is produced photochemically; a profile of the time constant for its production is given in figure 1. Above 40 km the time constant is less than 1 day and ozone is essentially in photochemical equilibrium. Below 30 km however, where most of the ozone in the atmosphere is located, ozone must clearly be influenced by both horizontal and vertical motions. This fact is illustrated by the observational data contained in figure 2 which exhibits the spring maximum in total ozone at high latitudes. Furthermore the absorption of solar radiation by ozone is an important stratospheric heat source which thus constitutes a feed-back mechanism to the stratospheric climatology.

Thus to successfully simulate the stratospheric ozone distribution, an interactive photochemical-dynamical model is required. Current large general circulation models are not easily adapted to the ozone problem because of the extensive computing time (currently several hours) required to make a 1 day simulation. In the ozone problem we must allow for an adjustment time of several years for the stratosphere and we should like to simulate the important seasonal variations therein. Furthermore since some stratospheric parameters are poorly known at the present time (e.g., certain chemical reaction rates) several runs of the model may be envisaged. Our model, which takes only 40 seconds for a 1 day simulation on an IBM 360/90, will be run several times, each run consisting of several annual cycles.

Because we are primarily interested in the stratosphere, for which there is evidence that smaller scale features are of secondary importance, our model incorporates a fairly limited horizontal resolution (by tropospheric standards). This is accomplished by using a fairly small number (79) of spherical harmonics for the horizontal representation of the dependent variables. In addition, the relative absence of energy in the shorter planetary and synoptic scale waves also permits a number of simplifications in the dynamic and thermodynamic representations. For example, we make use of the differentiated form of the motion equations and invoke the quasi-geostrophic approximation. The large-scale tropospheric motions responsible

for driving the stratosphere are included by allowing the model to extend downwards to the ground.

Trenberth (1973) successfully used a model of this type to study stratospheric warmings. Trenberth used only 9 levels in the vertical and 24 horizontal degrees of freedom without any chemistry but was able to reproduce realistic stratospheric warmings in late winter resulting from tropospheric forcing. A similar model which included a limited set of chemical reactions was used somewhat earlier by Clark (1970). Although Clark's model possessed even poorer resolution than Trenberth's, he was able to reproduce numerically the observed tendency for the large scale motion field to shift the maximum of vertically integrated ozone poleward from the low-latitude source region.

The principle features of our model consist of the inclusion of NO_x chemistry, together with the potential for adding additional chemistry at a later time, and the ability to simulate seasonal variations by running the model over several annual cycles. Without NO_x the model would overpredict the total amount of ozone in the atmosphere. This fact is evident in previous models in which certain assumptions (Hunt, 1969), subsequently proved false, or artificial adjustments (Clark, 1970) had to be made to reduce the total ozone amounts.

Model Equations

Using $\log_e$ (pressure) as the vertical coordinate, the model equations are:

$$R\nabla^2 T = \underline{\nabla}\cdot\left(f\underline{\nabla}\frac{\partial\psi}{\partial Z}\right)$$

$$\frac{\partial S}{\partial t} = \frac{\partial}{\partial t}\nabla^2\psi = -\overline{J}(\psi, S+f) - \underline{\nabla}\cdot\left(f\underline{\nabla}\frac{\partial\overline{\chi}}{\partial\overline{P}}\right) + \\ + \underline{\nabla}\cdot\left(\underline{F}_r \times \hat{\underline{k}}\right)$$

$$\frac{\partial\overline{T}}{\partial t} = -\overline{J}(\psi, T) - \overline{W}\left(\frac{d\overline{T}}{dZ} + \chi\overline{T}\right) + \frac{\dot{q}}{c_p}$$

$$\frac{\partial\chi_{O_3}}{\partial t} = -\overline{J}(\psi, \chi_{O_3}) - \overline{W}\frac{\partial\overline{\chi}_{O_3}}{\partial Z} + \left[\frac{1}{n_m}\frac{dn_{O_3}}{dt}\right]_c + \\ + \frac{\partial}{\partial\overline{P}}\left[-\frac{K_d}{H_0^2}P\frac{\partial\chi_{O_3}}{\partial Z}\right]$$

where:

- f = Coriolis parameter
- R = gas constant for air
- $\underline{\nabla}$ = horizontal gradient operator
- ψ = streamfunction
- T = temperature
- Z = $-\log_e$ (p/1000 mb) with p = pressure
- ζ = vertical component of vorticity = $\nabla^2\psi$
- $\underline{F}_r$ = frictional force
- $\hat{\underline{k}}$ = unit vector in the vertical direction

X is related to the rate of change of pressure by

$$\nabla^2 X = \frac{dP}{dt}$$

W = vertical advection velocity $(=\frac{1}{p}\nabla^2 X)$

$J(\psi,s)$ = Jacobian operator representing the horizontal advection of the variable "s" by the non-divergent part of the horizontal wind

t = time

κ = $1 - c_v/c_p$

q/c_p = rate of heating (°K/sec)

c_p = specific heat of air at constant pressure

χ_{O_3} = volume mixing ratio of ozone

$\left[\frac{1}{n_m}\frac{dn_{O_3}}{dt}\right]_c$ = net chemical production rate of ozone

K_d = a vertical austausch coefficient

H_O = a scale height (= 7 km)

and $\overline{(\ )}$ indicates the horizontal average value.

These equations have been obtained using a "quasi-geostrophic" balance applied to the horizontal equations of motion in an energetically consistent manner (Lorenz, 1960). The differentiated form of the thermal wind arises out of these quasi-geostrophic balance conditions with the introduction of hydrostatics. Mass continuity provides the essential relationship between W and the vertically integrated velocity potential, X. The last terms in the vorticity and thermodynamic energy equations represent dissipation due to frictional stress and diffusion, and forcing through all types of heating.

Computation of the vertical thermal advection has been simplified by replacing the temperature at each level by its global horizontal mean. Thus, the "stability" factor, constructed from observed annual temperatures, becomes a horizontally specified function varying with pressure only. We will no longer interpret the temperature prediction equation as forecasting global mean temperatures since we would expect little change, either with season or changes in the ozone chemistry.

A similar approach has been followed for the prediction of ozone mixing ratios. Here again we have simplified the calculations by using global mean ozone values but, in contrast to temperature, we must allow for time variations in the mean ozone profile. This is accomplished by taking the horizontal average of the ozone prediction equation written in flux form, giving

$$\frac{\partial \overline{\chi}_{O_3}}{\partial t} = \frac{\partial}{\partial P}\left[P\overline{W'\chi'_{O_3}}\right] + \left[\overline{\frac{1}{n_m}\left(\frac{dn_{O_3}}{dt}\right)}\right]_c + \frac{\partial}{\partial P}\left[-\frac{K_d}{H_o^2}P\frac{\partial \overline{\chi}_{O_3}}{\partial Z}\right]$$

where the primes indicate deviations from horizontal average values.

These model equations are specified in the vertical direction at 26 levels equally spaced in Z between the ground and approximately 70 km (or at roughly 3 km height intervals). In the horizontal direction, T, ζ, χ_{O_3} and W are expanded as series of spherical harmonics $Y_n^m(\theta,\phi)$ using planetary waves with maximum wavenumber 6 (m = 0, ±1, ±2, ±3, ±4, ±5, ±6) and 6 degrees of freedom in latitude. Y_7^0 is also

included giving 79 harmonics in total. The equations are solved for χ_{O_3}, T, and W at levels 2, 3, 4, ...,25 and for ζ(or ψ) at intermediate levels 1-1/2, 2-1/2, ..., 25-1/2.

Since our model requires that the "quasi-geostrophic" balance condition be maintained at all times, we must generate vertical motions which satisfy this criteria. Therefore, we make use of the spectral form of the three-dimensional vertical velocity equation obtained in the usual manner by eliminating time dependency through substitution among the reduced dynamical set of equations.

Frictional stress, diffusion, and boundary conditions

Horizontal diffusion is neglected and thus the frictional force incorporates the effect of vertical stresses ($\underline{\tau}$) with the stress being represented by a vertical eddy viscosity, K_m. At the ground the stress is defined using a surface drag coefficient in a manner practically equivalent to applying the standard Ekman boundary-layer theory to the lowest layer of the model. These conditions yield expressions of the form

$$\nabla \cdot (\underline{F}_r \times \hat{k}) = \frac{\partial (PF)}{\partial P}$$

$$F_j = -\frac{K_m}{H_o^2} \frac{\partial \nabla^2 \psi}{\partial z} \quad \text{for} \quad 1 \leq j \leq 25$$

and

$$F_{26} = -k_d \nabla^2 \psi_{25\frac{1}{2}}$$

and we set $k_d = 1.6 \times 10^{-6} (\text{sec}^{-1})$. Vertical diffusion of ozone is treated in a mathematically similar way and at the ground the vertical flux of ozone is specified in terms of the concentration (Galbally, 1971). Thus

$$K_d \frac{\partial \chi}{\partial z} = d \chi_{26}$$

and we set $d = .08$ cm/sec based upon the surface destruction rate calculations of Fabian and Junge (1970). It is assumed that the vertical diffusion coefficients for momentum and ozone (K_m and K_d) are the same. Two profiles of the diffusion coefficient are shown in figure 3. Curve A is similar to that used by Wofsy and McElroy (1973) to explain measurements of atmospheric methane in the upper stratosphere and mesosphere. The

basis for this profile is largely that gravity waves, which provide a likely mixing process (Lindzen, 1971), increase exponentially with height. At the lower levels of the model the diffusion coefficient was assumed to decrease from a value of $10^5 cm^2/sec$ at the ground to a value of $2 \times 10^3 cm^2/sec$ in the lower stratosphere. Preliminary runs of the model indicated that too much ozone was being transported out of the 10-15 km region at high latitudes thus producing smaller ozone concentrations there than the observational data indicated. This result is produced in the model because we are using a latitudinally invarient K_d which contains a minimum at about 18 km to account for the effect of the tropopause. However, there is actually a considerable variation of tropopause height with latitude and we have tried to correct for this deficiency by using diffusion profile B which contains a 10 km region around the tropopause in which the diffusion coefficient assumes the small value of $4 \times 10^3 cm^2/sec$.

The boundary conditions on W are that W vanishes at level 1 and that it is given by the orographic upslope motion at level 26,

$$W_{26} = \frac{1}{H_o} \hat{\underline{k}} \times \underline{\nabla} \Psi_{25\frac{1}{2}} \cdot \underline{\nabla} h$$

where h represents the surface orography. Northern Hemisphere orographic patterns are used in the model together with values defined by reflecting Northern Hemisphere heights into the Southern Hemisphere (see figure 4). This procedure permits us to obtain statistical results over a shorter space of time

(eg., we get 2 Northern Hemisphere winters every year). Additional boundary conditions are that $\overline{w'\chi_{O_3}'}$ is equal to zero at the ground and the flux of ozone at the top of the model (where ozone is in photochemical equilibrium) is equal to zero.

Model heating

The important heating processes in the stratosphere differ from those in the troposphere and accordingly the representation of heating in the model consists of 3 parts. Method I is used at heights above 30 km where heating consists of absorption of solar energy by ozone and long wave cooling by ozone and carbon dioxide. Ultraviolet absorption is computed explicitly in the model as an integral over the solar spectrum and as a function of the ozone column density and is satisfactorily averaged over the day (to approximately 5 percent accuracy) using the empirical expression

$$\bar{Q} = \frac{H}{2.05\pi} \left[Q(\psi_1) + Q(\psi_2) \right]$$

where $2H$ radians is the length of the day at any grid point, ψ_1 is the solar zenith angle at the hour angle corresponding to local noon $+H/4$, and ψ_2 is the solar zenith angle at the hour angle corresponding to local noon $+3H/4$. A similar technique is used to evaluate the photodissociation rates (to be discussed shortly). The radiative cooling in the stratosphere above 30 km is parameterized with a Newtonian cooling approximation using values (see figure 5) similar to those deduced by Dickinson (1973).

Heating in regions below 20 km, represented as Method II, is more complicated, in principle involving both latent heat release and sensible heat flux from the ground in addition to solar and infrared radiation. This heating term is parameterized in a linear form

$$\frac{q}{c_p} = h(Z)\ (T^* - T)$$

using values consistent with those of Trenberth (1972). The parameter h is essentially a Newtonian cooling coefficient (values used are indicated in figure 5) and T* is a hypothetical equilibrium temperature field empirically determined from estimates of the heating rate and observations of temperature in the troposphere and lower stratosphere in the Northern Hemisphere. The T* field thus determined is permitted to possess non-zonal variations in planetary wave numbers 1 and 2 and furthermore a sinusoidal variation of T* with solar declination is included. In the Southern hemisphere the Northern hemisphere T* field is used with a 6 month time lag.

In the 20-30 km region, a linear weighting of methods I and II is used to produce a smooth gradation between the upper and lower regions. An additional term is however added to Method I in this region corresponding to the absorption of infrared radiation emitted by the ground and absorbed by ozone in the 9.6 μ band. This corresponds to a heat source of approximately 1°K/day at equatorial latitudes at 25 km (Dopplick, 1970).

Model Chemistry

The set of chemical reactions included in our model is very limited. It consists of the Chapman reactions

$$O_2 + h\nu \xrightarrow{J_{O_2}} O + O \quad ; \quad \lambda < 2459\ \text{Å}$$

$$O + O_2 + M \rightarrow O_3 + M \quad ; \quad k_1 = 6.6 \times 10^{-35} e^{\frac{510}{T}}\ \text{cm}^6\ \text{sec}^{-1}$$
(GARVIN AND HAMPSON, 1973)

$$O_3 + h\nu \xrightarrow{J_{O_3}} O_2 + O \quad ; \quad \lambda < 11400\ \text{Å}$$

$$O + O_3 \rightarrow 2O_2 \quad ; \quad k_1 = 1.9 \times 10^{-11} e^{-\frac{2300}{T}}\ \text{cm}^3\ \text{sec}^{-1}$$
(GARVIN AND HAMPSON, 1973)

and the catalytic cycle of NO_x:

$$NO + O_3 \rightarrow NO_2 + O_2; \quad k_2 = 1.7 \times 10^{-12} e^{-\frac{1310}{T}}\ \text{cm}^3\ \text{sec}^{-1}$$
(SCHOFIELD, 1967)

$$NO_2 + O \rightarrow NO + O_2; \quad k_3 = 9.1 \times 10^{-12}\ \text{cm}^3\ \text{sec}^{-1}$$
(DAVIS, 1973)

$$NO_2 + h\nu \xrightarrow{J_{NO_2}} NO + O; \quad \lambda < 4000\ \text{Å}$$

In order to produce more realistic atmospheric heating rates above 50 km, the pair of reactions

$$OH + O \rightarrow O_2 + H \; ; \; k_4 = 5 \times 10^{-11}\ \text{cm}^3\ \text{sec}^{-1}$$

$$HO_2 + O \rightarrow O_2 + OH; \; k_5 = 6 \times 10^{-11}\ \text{cm}^3\ \text{sec}^{-1}$$
(KAUFMAN, 1969)

have been added. This set of reactions leads to a net ozone

production rate of

$$\left[\frac{1}{n_m}\frac{dn_{O_3}}{dt}\right]_c = 0.42\, J_{O_2} - \left(\frac{2K+d_{OH}}{L}\right)\left(\chi_{O_3} J_{O_3} + \chi_{NO_2} J_{NO_2}\right)$$

where

$$K = k_1 \chi_{O_3} + k_3 \chi_{NO_2}$$

$$d_{OH} = k_4 \chi_{OH} + k_5 \chi_{HO_2} \simeq 4 \times 10^{-12} (n_m)^{-\frac{1}{2}}$$

and $L = .21\, \ell_1\, n_m$. The chemical reactions are temperature sensitive, particularly that between O and O_3, and thus react to temperature provided by the dynamics.

Many other reactions could have been included in our model but at the price of additional computer time and of considerable delay in obtaining results. The most significant omission is probably nitric acid which if included would require the addition of several odd nitrogen species. We are considering this problem as well as the possibility of adding a prediction equation for NO_x. However, the model results which follow are based upon OH and NO_2 profiles (see figure 6) which are similar to the results of one dimensional model calculations by McElroy et al (1973) and by McConnell and McElroy (1973) and which are assumed to be independent of latitude. The OH distribution above 45 km has a significant effect on the ozone distribution as does the distribution of NO_x between 20 km and 50 km.

The spectral representation of the ozone generation (and of heating by ozone) is a special problem because of the

trancendental functions involved. For this purpose we have designed an especially efficient transform procedure similar to that presented by Machenhauer and Rasmussen (1972). For this purpose the spectral data representing the predicted temperature and the ozone mixing ratio is transformed to a carefully selected grid mesh. The location and number of these grid points is determined in such a way as to guarantee an exact quadrature transformation to at least second degree. The heating and generation terms are then calculated at the grid points and the results are transformed back into the spectral domain, again retaining second degree accuracy. This procedure also has the property of eliminating aliased modes generated by the grid point calculation.

Initial conditions and numerical procedure

Initially the temperature field is set equal to a Standard Atmosphere temperature profile and the stream functions are set equal to zero. The model is started up from 44 days prior to the Spring equinox (i.e., early February) and a model year is 12 months, each month consisting of 30 days. The mean ozone distribution during the first few days of the model run, during which the dynamics has had little time to develop, is shown in figure 7. This initial ozone distribution is based upon the results of 1 dimensional model calculations. Using the chemistry and the vertical austausch coefficient of our global model an equilibrium calculation was made at several latitudes for a solar declination angle of 0° using the Standard Atmosphere temperature profile. The resulting profiles were then area weighted to produce the global mean ozone profiles depicted in figure 7. This figure shows the ozone distribution resulting from the prescribed NO_2 profile as well as the effect of omitting NO_x entirely. It is to be noted that an integration time of the order of 2 years is required for the tropospheric values to attain their equilibrium values. The figure also shows a mean mid-latitude profile compiled by Krueger and Mintzner (1973) based upon the limited number of rocket observations that have so far been made. There is excellent agreement between the predictions of the 1 dimensional model and the rocket observations except below the tropopause where large-scale transports through the tropopause involving tropospheric dynamics are likely to affect the profiles. At heights above 37 km the predictions

of the 1 dimensional model for each latitude were inserted in the 3 dimensional model as initial conditions while for heights below 37 km where large scale transports are expected to be important, the global mean value of ozone was inserted at each latitude and longitude.

The numerical integration of the global model makes use of the N-cycle time differencing scheme of Lorenz (1971) with one hour time steps. N is taken as 4. At the upper levels of the model the chemical time constants, as shown in figure 1, are very fast and would lead to numerical instabilities for our time increment. However, because of these relatively fast time constants, photochemical equilibrium can be safely assumed for heights above 50 km. In practice we update χ_{O_3} diagnostically via the photochemical equilibrium assumption at each time step for levels 9 and above (i.e., above 47 km). This procedure overemphasises the reaction of ozone to temperature perturbations at the upper levels, but on the basis of test runs it appears that the dynamics of the stratosphere and mesosphere are little affected by this assumption.

The initial distribution of heating (actually averaged over the first 2 days) is shown in figure 8. The long wave cooling is initially zero because $T = \bar{T}$ and the global mean value of temperature has been omitted from the heating because $\bar{T}$ is not predicted. Thus in the stratosphere and mesosphere the initial latitudinal heating gradients are due entirely to heating by ozone. In the troposphere the initial heating distribution is in a sense a map of T^* at 44 days before the Spring equinox (T^*, however, also possesses a non-zonal component).

Model results

Several 96 day runs have been made with the model during the past few months. These runs were made in an attempt to discover how the dynamics of the model varied as a function of certain parameters, thus eliminating the need for additional full-scale runs of the model. Two full 3 year runs of the model have been made; the initial analysis of the results of the second run is presented as the remainder of this paper. The difference between the second integration (run 12) and the first (Cunnold et al, 1974) is that run 12 contains orographic effects and an adjustment in the static stability to crudely account for the release of latent heat. Also, a coding error related to the frictional drag at the lower boundary has been corrected.

(a) dynamics

After an initial zonal build-up period of about 28 days, the eddies become active and the kinetic energy begins to stabilize at about 250 m^2/sec^2. The level of available potential energy is about 2.5 times that of the kinetic energy. These values are generally in agreement with the results of other models.

Average zonal wind profiles for seasons 10 and 11 are shown in Figs. 9 and 10. For comparison, observations analysed by Newell (1969) for summer and winter have been reproduced on the upper half of Fig. 9. We see that for season 10 (the winter-summer situation) the model shows the presence of a high-level wind maximum similar to the polar night jet in winter and

easterlies in summer. The magnitude of the westerly wind maximum is about 80 m/sec at 50 km in excellent agreement with Newell's data. At higher levels the failure of this maximum to close off is probably the result of the artificial boundary of the model at 70 km. The 50-70 km region in our model is in essence a lid which is needed in order to obtain the correct dynamics at lower altitudes. By forcing W to zero, the artificial lid at 72 km probably prevents the creation of a cold mesosphere over the summer pole, which must be associated with the decrease in zonal wind speeds above 50 km observed in the real atmosphere. (This conclusion agrees with the results of Leovy (1964) in his test of different upper boundary conditions. Compare his figures 5 and 12).

The location of the wintertime wind maximum at 40°N is in excellent agreement with the observations. The strength and location of the summertime easterlies also agrees well with the observations except perhaps above 50 km where again the upper boundary may be affecting the results. In the troposphere a jet of the correct amplitude is obtained in the winter. It is located somewhat too close to the equator, however, and in fact extends right across the equator. This result was probably to be expected because our model does not possess the baroclinically active waves of higher wavenumbers than 6 which also transport momentum from equatorial to mid-latitudes. In the lower troposphere our model gives equatorial easterlies and a belt of westerlies in mid-latitudes. The surface winds obtained in run 12 are in much better agreement with the observations

than were the surface winds of the earlier run (run 10). This is because run 10 contained a coding error in the computer program which resulted in the use of ψ at level 24 1/2 (rather than level 25 1/2) in computing F_{26}. During the equinoctial seasons (Fig. 10), the zonal wind profile obtained by the model shows the transition state for hemispheric season reversal.

Zonal temperature distribution both as obtained from observations and given by our model are shown in figure 11. Here it is interesting to note that in the lower stratosphere (about 17-20 km) the model temperature fields exhibit a poleward increase, similar to the observations. Elsewhere, as expected, temperature decreases from equator to pole with the exception of the summer upper stratosphere. In comparing the model results with observations the model seems to slightly overpredict the pole to pole temperature gradient in the solstitial stratosphere. This could be related to the "lid" at 72 km or might be the result of a slightly excessive pole to pole ozone gradient in the upper stratosphere caused by our inadequate knowledge of the latitudinal distribution of other minor constituents.

The meridional circulations for seasons 10 and 11 are shown in figure 12. The three cell hemispheric circulation in the troposphere changing over to a two cell circulation in the stratosphere is clearly evident at all seasons except during the summer when the circulation is very weak and not well established. The strong cross-equatorial transports from the summer to the winter hemisphere should also be noted. Figure 13 shows some mean

stratospheric circulations in January and March according to Vincent (1968). We see that our results are in general agreement with those of Vincent (except for the January, 1965 observations which show a 3 cell pattern in the stratosphere at that time). In the troposphere the ITCZ possesses an annual oscillation with its location varying between 10°N and 10°S. The circulation of the equatorial troposphere has been compared with the flux data of Newell et al (1972) and found to possess excellent agreement. For example, in winter the model shows a maximum of just over 200 tons/second being transported equatorward by the equatorial Hadley cell between the ground and 6 km altitude. Corresponding values by Newell average to just under 200 tons/second for the same conditions.

Monthly average maps of geopotential height for September and December at 10 mb are shown in figure 14. These maps show clearly the lack of standing wave activity in the summer (approximately zonal flow), the presence of wave numbers 1 or 2 in the winter, and the existance of an Aleutian high at 180° longitude in December. These features are apparently related to the ability of certain tropospheric standing waves to propagate upwards high into the stratosphere in the presence of westerly flow throughout the troposphere and stratosphere. On the other hand, upward propagation of these waves is not possible through a layer in which low-level westerlies reverse to easterly flow aloft.

There is evidence for the occasional occurrence of large and rapid stratospheric temperature changes in our model. For example at 2 mb and 70° latitude temperature changes in excess of 45°K are found to occur during the spring over the period of approximately 1 week. At 10 mb the amplitude of the temperature changes is approximately 20°K. Although the details are not shown here, the warmings appear to propagate westward with time and may occur several days later at the 10 mb level than at the higher 2 mb level. A full analysis of the stratospheric warmings in our model will be undertaken shortly.

(b) Ozone results

The global mean ozone profile calculated for year 3 is shown in figure 15. During year 2 ozone decays approximately 10 percent in value for levels below 18 (approximately 22 km); in year 3 however ozone appears to possess only an annual variation.

The global average contributions of dynamics and diffusion to the upward flux of ozone for season 10, month 2 (June) is shown in figure 16. Similar profiles are obtained in equinoctial months. The maximum net production of ozone occurs at level 15 from which the ozone is transported downwards by diffusion with some compensating upward motion from the large scale dynamics between levels 15 and 18. There is therefore somewhat less ozone in the lower stratosphere after a 2 year integration than there was initially. The large scale dynamics is apparently able to transport approximately 20 tons/second of ozone through

the tropopause, and the total flux of ozone being destroyed at the ground is about 30 tons/second. This is in close agreement with the global surface destruction estimates by Fabian and Junge (1970). The downward flux in the upper troposphere has considerably reduced the ozone concentration in the 10-15 km region relative to its initial concentration (compare figure 7) while substantially adding to that below 10 km. It is particularly encouraging that we are obtaining the observed ozone concentration at the ground while using a lower boundary condition which in no way fixes the value there.

The model seems to be ending up with not quite enough ozone in the 10-15 km region. This result may be examined in more detail in the lower parts of figures 17 and 18 which show the predicted latitudinal distribution of ozone concentration. The figures may be compared against the observations analysed by Hering and Borden (1964, 1965 and 1967), presented here in the upper parts of figures 17 and 18. We note that there is good agreement between the model results and the observations, with ozone being transported poleward and downward. The ozone deficiency between 10 and 15 km now shows up primarily at high latitudes in winter and spring. Calculations suggest that this result could be modified by reducing the diffusion coefficient in the 10 to 15 km height range which would reduce the tendency for ozone to be diffused out of the polar lower stratosphere. It is also possible that use of a more realistic NO_2 distribution would accomplish this objective.

At altitudes above 30 km the model predictions regarding ozone may be compared with the satellite observations which are just beginning to appear in print. A sample of that data is shown as figure 19 from Krueger et al, 1973. Figure 20 shows the predicted distribution of ozone mixing ratios for season 8 (winter-summer). The observed ozone distributions contained in figure 19 are supposed to be typical of particular seasons and thus figure 20 may be directly compared with orbit 938 (for June 17). Agreement between observations and model results is excellent with the model exhibiting peak mixing ratios centered around the subsolar point, and a secondary peak at high altitudes in the winter hemisphere associated with the cold temperatures there. The model predictions above level 10 at high latitudes of the winter hemisphere are inexact because of the small solar illumination and the diagnostic nature of the ozone prediction there.

The predicted latitudinal variation of total ozone as a function of the time of year averaged over year 2 and is presented in figure 21. Comparable observed data from Dutsch (1969) is also shown. The model results clearly show a spring maximum in total ozone at all latitudes with the largest concentrations occurring at high latitudes in good qualitative agreement with the observations. However the pole to equator gradients and the seasonal variations are somewhat weaker than observed. This feature is probably also related to the shortage of ozone in high latitudes in the 10-15 km region. Figure 22

depicts the latitudinal distribution of the contributions of the meridional circulation and eddy motions to the horizontal fluxes of ozone for the middle months of seasons 10 and 11 (September and December). At mid-latitudes the meridional transports are always equatorward while the eddy transports are always poleward with the largest transports occurring in the winter and the spring, with only small transports occurring in the summer. The eddy fluxes appear to possess the anticipated seasonal variation and to have a mean value in good agreement with the observed value of 50 tons/second reported by Hutchings and Farkas (1971) for a single mid-latitude station. The large transequatorial fluxes due to the meridional circulation during summer and winter may also be noted and correspond to the large cross equatorial transports of tropospheric air at that time of year.

The predictions of the model relating to the global distribution of columnar ozone for each season are presented in figure 23. The results may be compared against the observations analysed by Wu (1973) of which the monthly mean values for 1960-1969 for the mid-months of each season are given as figures 24a-24d. There is good agreement between theory and observation for the location of the various features of the ozone distribution particularly during the solsticial seasons. In particular the extensive region of generally low ozone concentrations during summer centered at approximately 120°E and 70°S is also present in Wu's charts, as is the region of high ozone concentrations centered at North American latitudes. In the winter the extensive region of high ozone concentrations between approximately 100°E and 30°W bears a remarkable

resemblance to the region of high ozone concentrations found in Wu's data including a peak concentration in approximately the same location. The model also exhibits a small high in the neighborhood of Arosa (20°E).

The magnitude of the fluctuations in columnar ozone are presented in figure 25 where they are compared against ground-based observations in the northern hemisphere summarized by Newell (1963). Both the model results and the observations possess an average standard deviation of 30 m. atm. cm. at mid-latitudes. The variation of the predicted fluctuations with latitude is however less strong than the variation of the observed fluctuations. This result is almost certainly associated with the weaker pole to equator gradient of total ozone that the model results possess. On the other hand the seasonal variation of the variance is in good agreement with the observations.

Correlations between total ozone and several other parameters have been calculated. Total ozone is found to be negatively correlated with the 700 mb temperature with a correlation coefficient of approximately -0.5 at mid-latitudes in winter. On the other hand it is positively correlated with the 100 mb temperature with a correlation coefficient of +0.4. These correlations are similar to values quoted in Craig's book (1965) based upon observations at Oxford. The correlation coefficients between columnar ozone and ozone concentrations at particular pressure levels have also been calculated. The results show a peak correlation of approximately 0.6 at mid-latitudes at around 15 km in good agreement with the data of Hering and Borden (1967).

The model results do not however exhibit the fairly rapid decrease of correlation coefficient with height above 15 km. For example, a correlation coefficient of 0.3 is still found in the model results up to 30 km altitude.

Conclusions

The model appears to be performing well for the purpose for which it has been designed. The model is simulating the dynamics of the stratosphere very well giving in the winter a westerly wind maximum of the observed amplitude and location which changes over to easterlies in summer. Furthermore, the lower stratosphere is being forced by the troposphere while the troposphere and the upper stratosphere are largely forced by the in-situ distribution of heating and cooling.

The agreement between data on atmospheric ozone and the predictions of the model is generally excellent. In particular the model shows ozone to be transported polewards and downwards and the poleward eddy flux is of the same magnitude as is observed. Moreover, the general level of fluctuations of columnar ozone are correctly predicted as is the seasonal variation in ozone at mid-latitudes. The standing wave patterns of columnar ozone also seem to agree well with the observations. The only significant deficiency in the model is that the pole to equator gradients of ozone are not as large as those observed particularly during the winter and the spring. An attempt is underway to remove this deficiency by adding a realistic latitudinal distribution of NO_2 and by reducing the diffusion coefficient (perhaps to zero) everywhere except in the atmospheric boundary layer.

Acknowledgement

This research was supported as part of its Climatic Impact Assessment Program by the U.S. Department of Transportation, contract no. AT 11-1-2249. We also gratefully acknowledge the computer time provided by the Goddard Institute for Space Studies, New York City, through Grant NGR 22-009-727 from the National Aeronautics and Space Administration.

References

Clark, J., 1970: A quasi-geostrophic model of the winter stratospheric circulation. Mon. Wea. Rev., 98, 443-461.

Craig, R.A., 1965: The Upper Atmosphere meteorology and physics, Academic Press, New York, pp. 209.

Cunnold, D., F. Alyea, N. Phillips, and R. Prinn, 1974: A general circulation model of stratospheric ozone. Paper presented at IAMAP/IAPSO Symposium, Melbourne, Australia, Jan. 14-26.

Davis, D.D., 1973: New rate measurements on the reaction of O(3P), O_3 and OH, Paper presented at AIAA/AMS International Conference on the Environmental Impact of Aerospace Operations in the High Atmosphere, Denver, Colorado, June 11-13, Paper no. 73-501.

Dickinson, R., 1973: A method of parameterization for infrared cooling between altitudes of 30 and 70 km. J. Geophys. Res., 78, 4451-4457.

Dopplick, T.G., 1970: Global radiative heating of the earth's atmosphere, M.I.T. Meteorology Department, Report no. 24, April 15.

Dutsch, H.U., 1969: Atmospheric ozone and ultraviolet radiation. World Survey of climatology, 4 (ed., H.E. Landsberg, Elsevier Publishing Co., Amsterdam).

Fabian, P., and C. Junge, 1970: Global rate of ozone destruction at the earth's surface. Arch. Meteor., Geo., Bioklimat., (a)-Meteor. u. Geo., 19, 161.

Galbally, J., 1971: Ozone profiles and ozone fluxes in the atmospheric surface layer. Quart. J. Roy. Meteor. Soc., 97, 18.

Garvin, D., and R.F. Hampson, 1973: Atmospheric modelling and the chemical data problem. Presented at AIAA/AMS Internationl Conference on the Environmental Impact of Aerospace Operations in the High Atmosphere, Denver, Colorado, June 11-13, Paper no. 73-500.

W.S. Hering and T.R. Borden, Jr., 1964: Ozonesonde Observations Over North America, 2, Environmental Research Papers No. 38, AFCRL-64-30(II).

W.S. Hering and T.R. Borden, Jr., 1965: Ozonesonde Observations Over North America, 3, Environmental Research Papers No. 133, AFCRL-64-30(III).

W.S. Hering and T.R. Borden, Jr., 1967: Ozonesonde Observations Over North America, 4, Environmental Research Papers No. 279, AFCRL-64-30(IV).

Hunt, B., 1969: Experiments with a stratospheric general circulation model: III. Large-scale diffusion of ozone including photochemistry. Mon. Wea. Rev., 97, 287-306.

Hutchings, J., and E. Farkas, 1971: The vertical distribution of atmospheric ozone over Christchurch, New Zealand. Quart. J. Royal Meteor. Soc., 97, 249-254.

Justus, C.G., 1973: Upper atmosphere mixing by gravity waves. Presented at the AIAA/AMS International Conference on the Environmental Impact of Aerospace Operations in the High Atmosphere, Denver, Colorado, June 11-13, 1973, Paper no. 73-495.

Kaufman, F., 1969: Neutral reactions involving hydrogen and other minor constituents. Can. J. Chem., 47, 1917-1924.

Krueger, A.J., D.F. Heath, C.L. Mateer, 1973: Variations in the stratospheric ozone field inferred from nimbus satellite observations. Pure Appl. Geophys., 106-108, 1254-1263.

Krueger, A., and R. Minzer, 1973: A proposed mid-latitude ozone model for the U.S. Standard Atmosphere. Goddard Space Flight Center, X-651-73-72.

Leovy, C., 1964: Simple models of thermally driven mesospheric circulation. J. Atmos. Sci., 21, 327-341.

Lindzen, R.S., 1971: Tides and gravity waves in the upper atmosphere, In Mesospheric Models and Related Experiments, ed, G. Fiocco, D. Reidel : Dordrecht, Holland, p. 122.

Lorenz, E.N., 1960: Energy and numerical weather prediction, Tellus, 12, 364.

Machenhauer, B., and E. Rasmussen, 1972: On the integration of the spectral hydrodynamical equations by a transform method. Report No. 3, Institute for Theoretical Meteorology, Copenhagen University, 44 pp.

McConnell, J.C., and M.B. McElroy, 1973: Odd Nitrogen in the Atmosphere. J. Atmos. Sci., 30, 1465-1480.

McElroy, M., S. Wofsy, J. Penner, J. McConnell, 1973: Atmospheric ozone: possible impact of stratospheric aviation. J. Atmos. Sci., 31, 287-303.

Newell, R.E., 1963: Transfer through the tropopause and within the stratosphere. Quart. J. Royal Meteor. Soc., 89, 167-204.

Newell, R.E., 1969: Radioactive contamination of the upper atmosphere, Progress in Nuclear Energy - Series XII, Health Physics, Vol. 2, ed. A.M. Francis Duhamel, Pergamon, Oxford, 535-550.

Newell, R.E., J.W. Kidson, D.G. Vincent, and G.J. Boer, 1972: The general circulation of the tropical atmosphere and interaction with extratropical latitudes, Vol. 1, M.I.T. Press, Cambridge, Mass., p. 45.

Schofield, K, 1967: An evaluation of kinetic rate data for reactions of neutrals of atmospheric interest. Planet. Space Sci., 15, 643.

Trenberth, K., 1972: Dynamic coupling of the stratosphere with the troposphere and sudden stratospheric warmings. Ph.D. Thesis, Dept. of Meteorology, MIT, Jan. 1972.

Vincent, D.G., 1968: Mean meridional circulations in the Northern Hemisphere lower stratosphere during 1964 and 1965, Quart. J. Royal Meteor. Soc., 94, 333-349.

Wofsy, S., and M. McElroy, 1973: On vertical mixing in the upper stratosphere and lower mesosphere. J. Geophys. Res., 78, 2619-2624.

Wu, M-F, 1973: Observations and analysis of trace constituents in the stratosphere. Annual Report, Contract no. DOT-05-20217, July, Environmental Res. Tech., 429 Marrett Rd., Lexington, Mass. 02173.

Figure Captions

Fig. 1. Time constants for the chemistry and vertical diffusion of ozone.

Fig. 2. Total ozone distribution with season and latitude (from Dutsch, 1969)(10^{-3} cm or Dobson units).

Fig. 3. Vertical diffusion coefficients used in the model.

Fig. 4. Model surface topography in decameters.

Fig. 5. Newtonian cooling coefficients used in the model.

Fig. 6. Latitudinally independent OH and NO_2 profiles assumed in the model.

Fig. 7. The global average ozone distribution predicted initially in the model based upon a one-dimensional calculation.

Fig. 8. The heating distribution for days 0 to 2 (at 44 days prior to the spring equinox).

Fig. 9. Vertical cross-section of the zonal wind for season 10 (m/sec) compared with the summer-winter observations analysed by Newell (1969).

Fig. 10. The vertical cross-section of the zonal wind for season 11.

Fig. 11. The atmospheric temperature distribution obtained for season 10 compared against the observed atmospheric temperature distribution for summer and winter according to Newell (1969).

Fig. 12. The mean meridional circulations for seasons 10 and 11.

Fig. 13. January and March mean meridional circulations in the stratosphere according to Vincent (1968).

Fig. 14. Mean height deviations (decameters) for seasons 10 and 11, month 2 at approximately 10 mb.

Fig. 15. The predicted global mean ozone profile for year 2 as a function of height and its comparison with mid-latitude rocket data presented by Krueger and Mintzer (1973).

Fig. 16. The contributions of diffusion and large scale dynamics to the vertical motion of ozone for season 10.

Fig. 17. The distribution of ozone as a function of latitude and height predicted for season 10 compared against the mean observed ozone density (10^{11} molecules/cm^3) for summer and winter derived from the ozone profile data obtained by Hering and Borden (1964, 1965, and 1967) (from Wu, 1973).

Fig. 18. The distribution of ozone as a function of latitude and height predicted for season 11 compared against the mean observed ozone density (10^{11} molecules/cm^3) for fall and spring derived from the ozone profile data obtained by Hering and Borden (1964, 1965, and 1967) (from Wu, 1973).

Fig. 19. Pseudo-meridional cross-sections of ozone mass mixing ratio derived from BUV data during four orbits of Nimbus 4 (from Krueger et al, 1973).

Fig. 20. Zonal mean ozone mixing ratios (μgm/gm) as a function of latitude and height predicted for season 8.

Fig. 21. Total ozone distribution with season and latitude averaged over years 2 and 3 and compared against ozone observations from Dutsch (1969).

Fig. 22. The contributions of the meridional circulation and the eddies to the horizontal transport of ozone for the mid-months of seasons 10 and 11.

Fig. 23. Predicted distribution of total ozone for seasons 10 and 11 (10^{-3} cm)

Fig. 24a. Distribution of total ozone in the Northern Hemisphere for March, based on 11 years of data, from Wu (1973).

Fig. 24b. Distribution of total ozone in the Northern Hemisphere for June, based on 11 years of data, from Wu (1973).

Fig. 25c. Distribution of total ozone in the Northern Hemisphere for September, based on 11 years of data, from Wu (1973).

Fig. 24d. Distribution of total ozone in the Northern Hemisphere for December, based on 11 years of data, from Wu (1973).

Fig. 25. The latitudinal variation of the standard deviations of total ozone as a function of season and compared against observations reported by Newell (1963). Units are 10^{-3}cm.

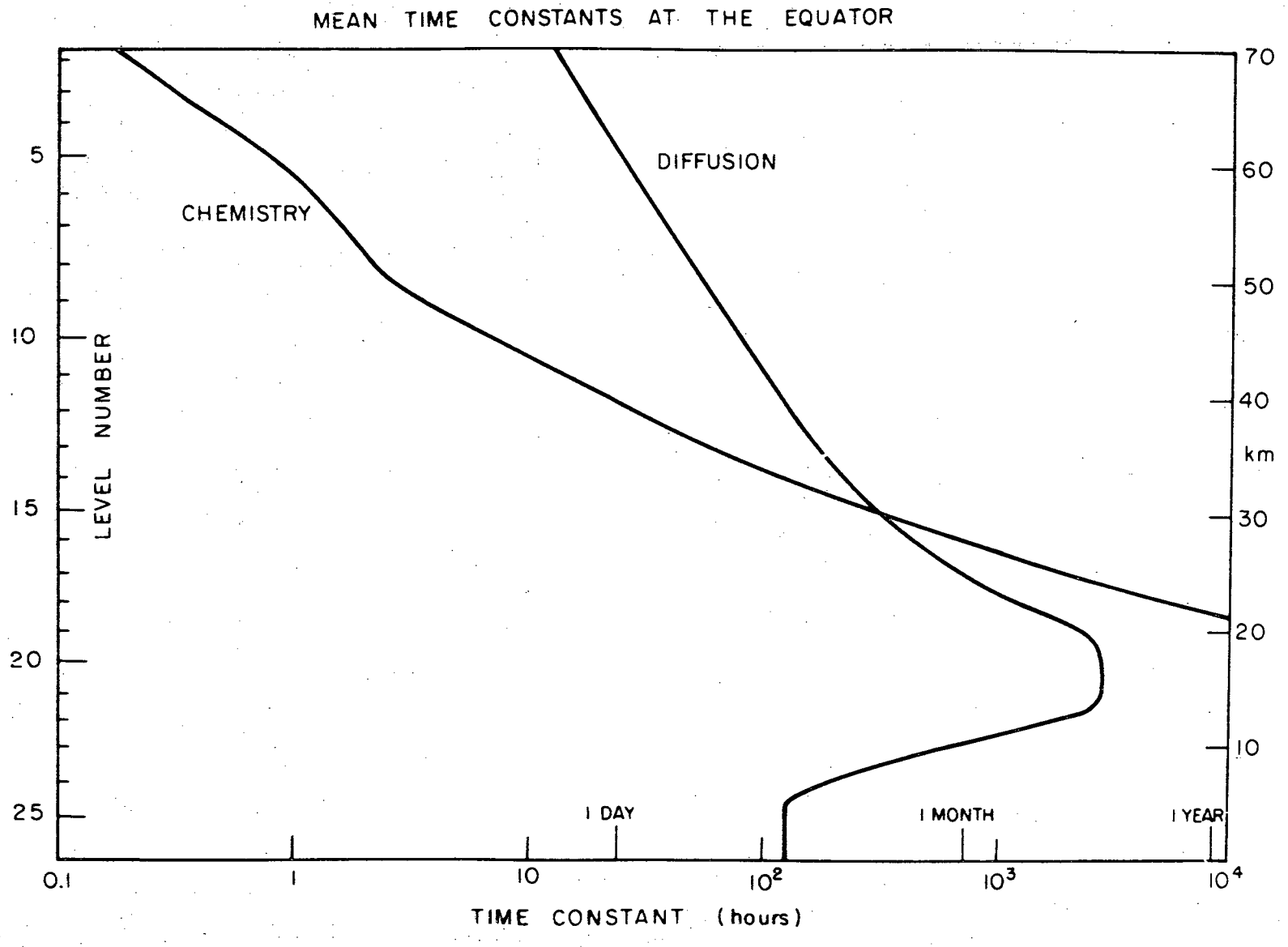
MEAN TIME CONSTANTS AT THE EQUATOR
DIFFUSION
CHEMISTRY
LEVEL NUMBER
5
10
15
20
25
70
60
50
40
km
30
20
10
1 DAY
1 MONTH
1 YEAR
0.1
1
10
10^2
10^3
10^4
TIME CONSTANT (hours)

Fig. 1.

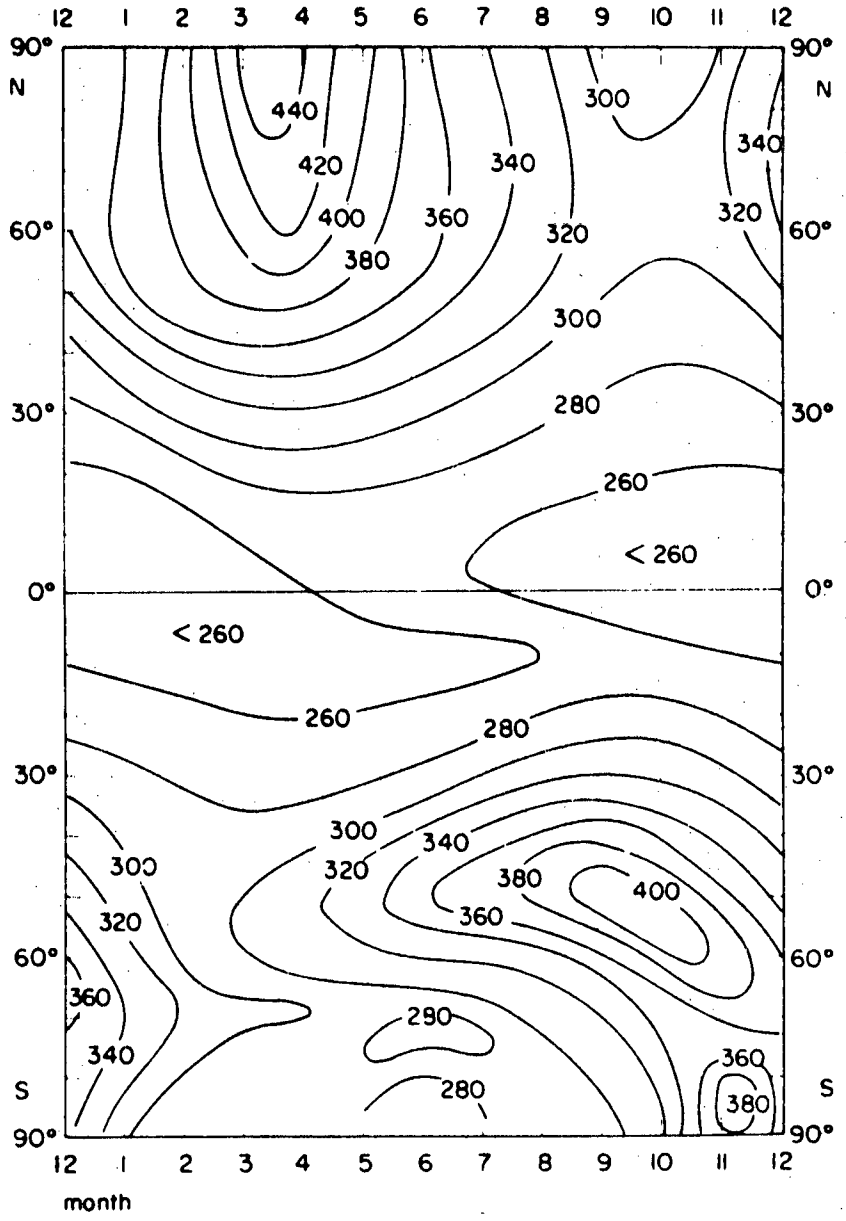
12 1 2 3 4 5 6 7 8 9 10 11 12
90° N
60°
30°
0°
30°
60°
S 90°
440
420
400
380
360
340
320
300
280
260
< 260
< 260
260
280
300
320
340
360
380
400
300
320
360
340
290
280
360
380
month

Fig. 2.

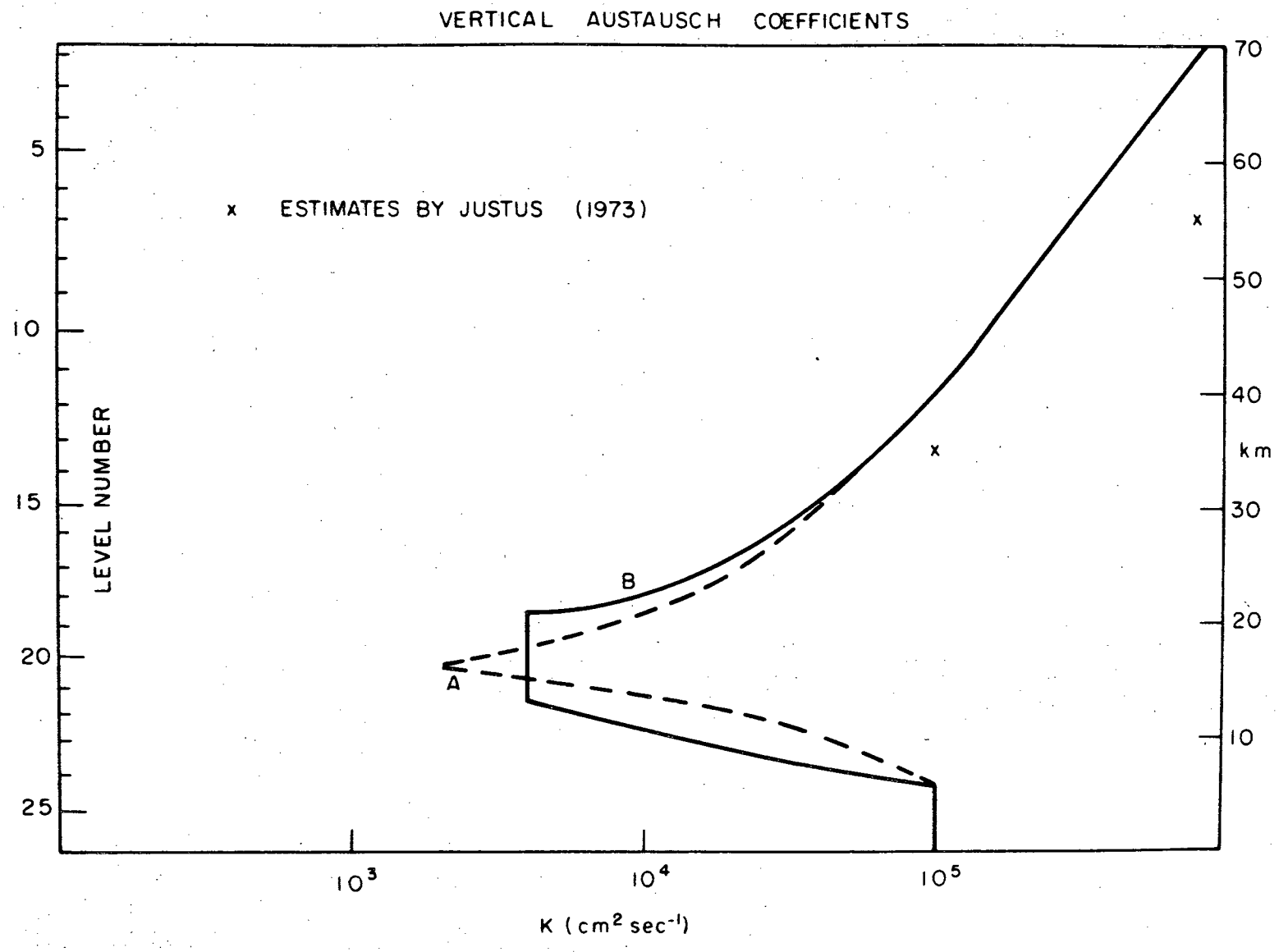
VERTICAL AUSTAUSCH COEFFICIENTS
x ESTIMATES BY JUSTUS (1973)
LEVEL NUMBER
5
10
15
20
25
70
60
50
40
30
20
10
km
B
A
10^3
10^4
10^5
K ($cm^2 sec^{-1}$)

Fig. 3.

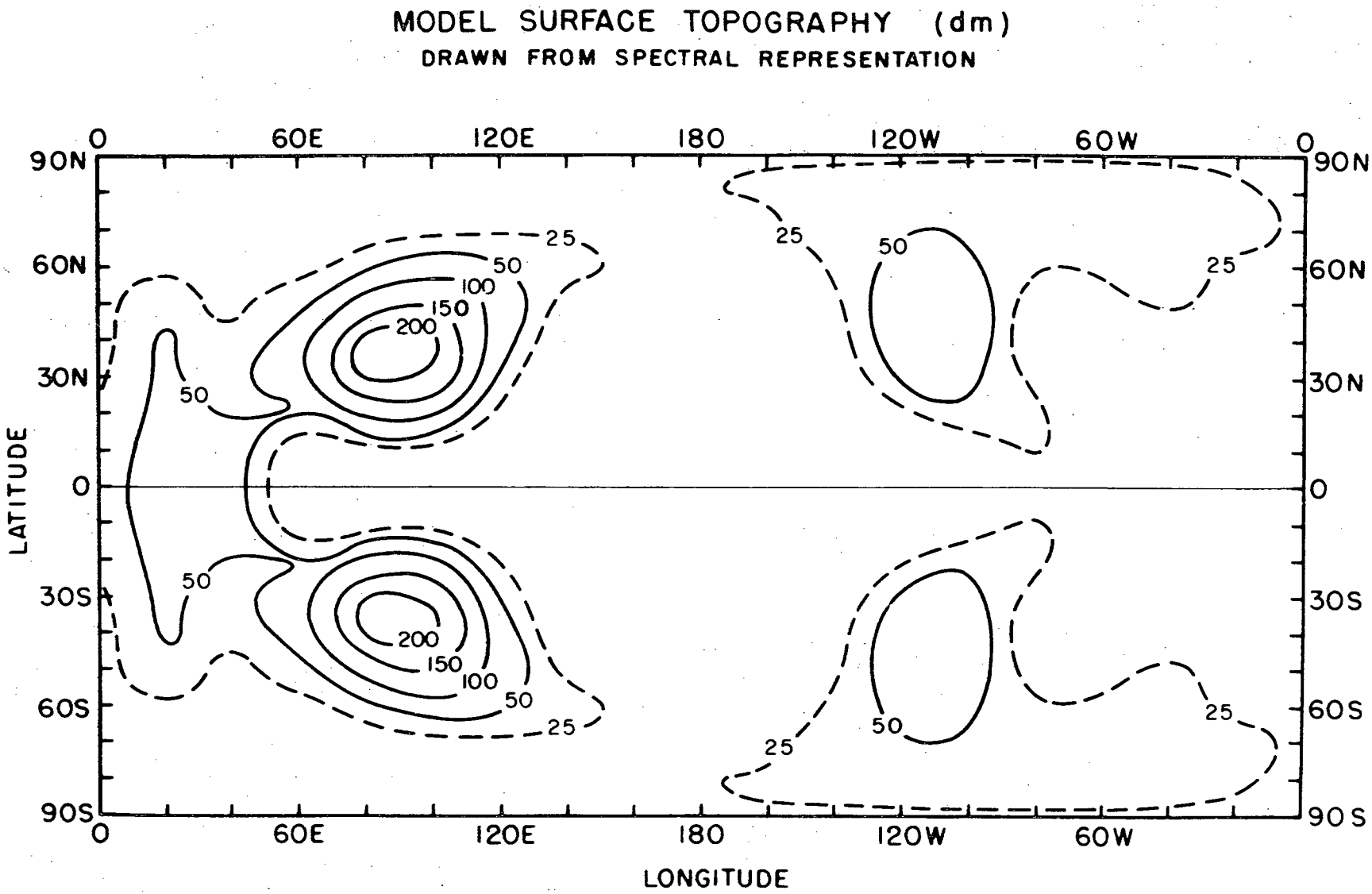
MODEL SURFACE TOPOGRAPHY (dm)
DRAWN FROM SPECTRAL REPRESENTATION
0
60E
120E
180
120W
60W
0
90N
60N
30N
0
30S
60S
90S
LATITUDE
LONGITUDE
25
50
100
150
200

Fig. 4

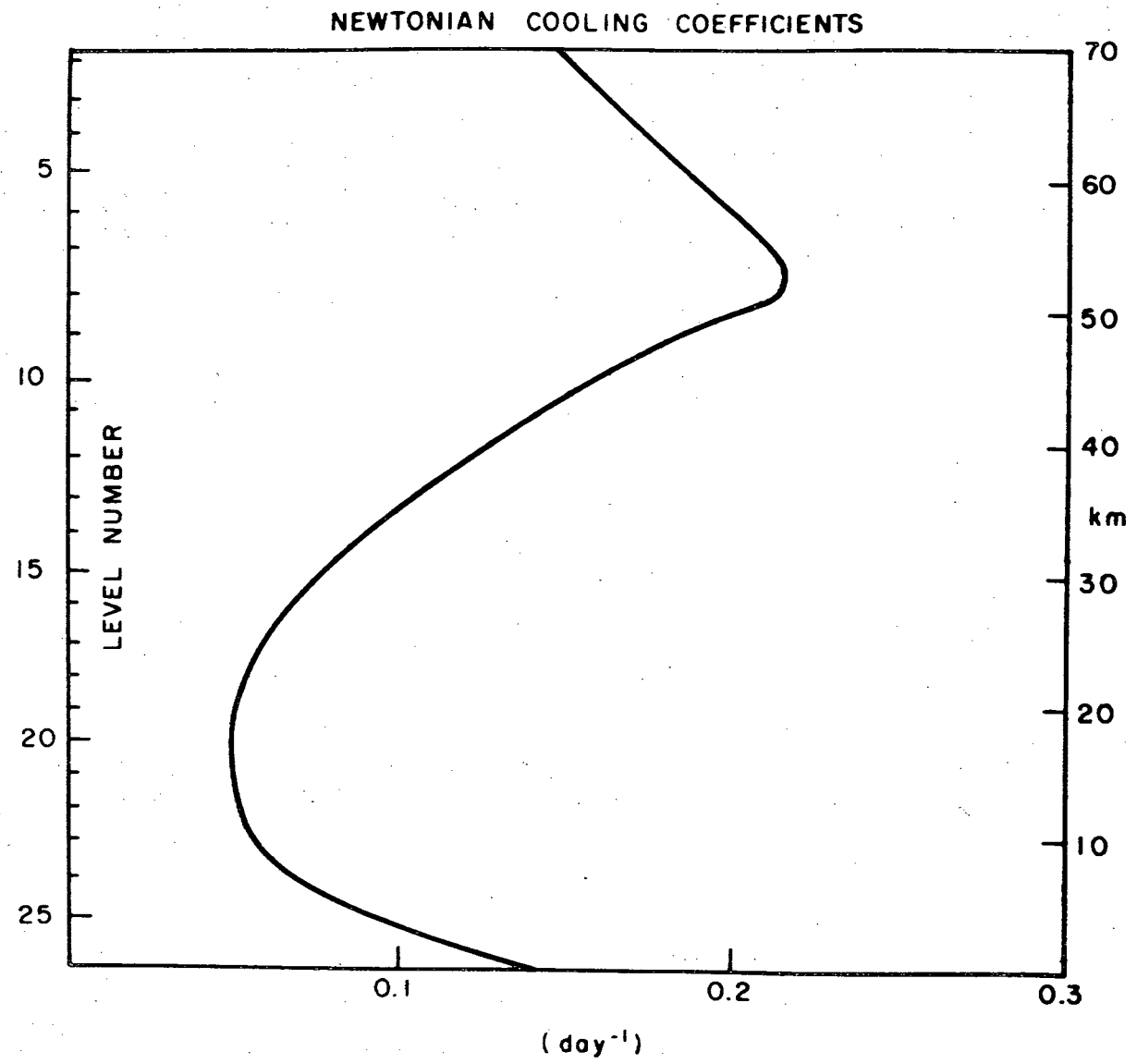
NEWTONIAN COOLING COEFFICIENTS
LEVEL NUMBER
5
10
15
20
25
70
60
50
40
km
30
20
10
0.1
0.2
0.3
(day⁻¹)

Fig. 5.

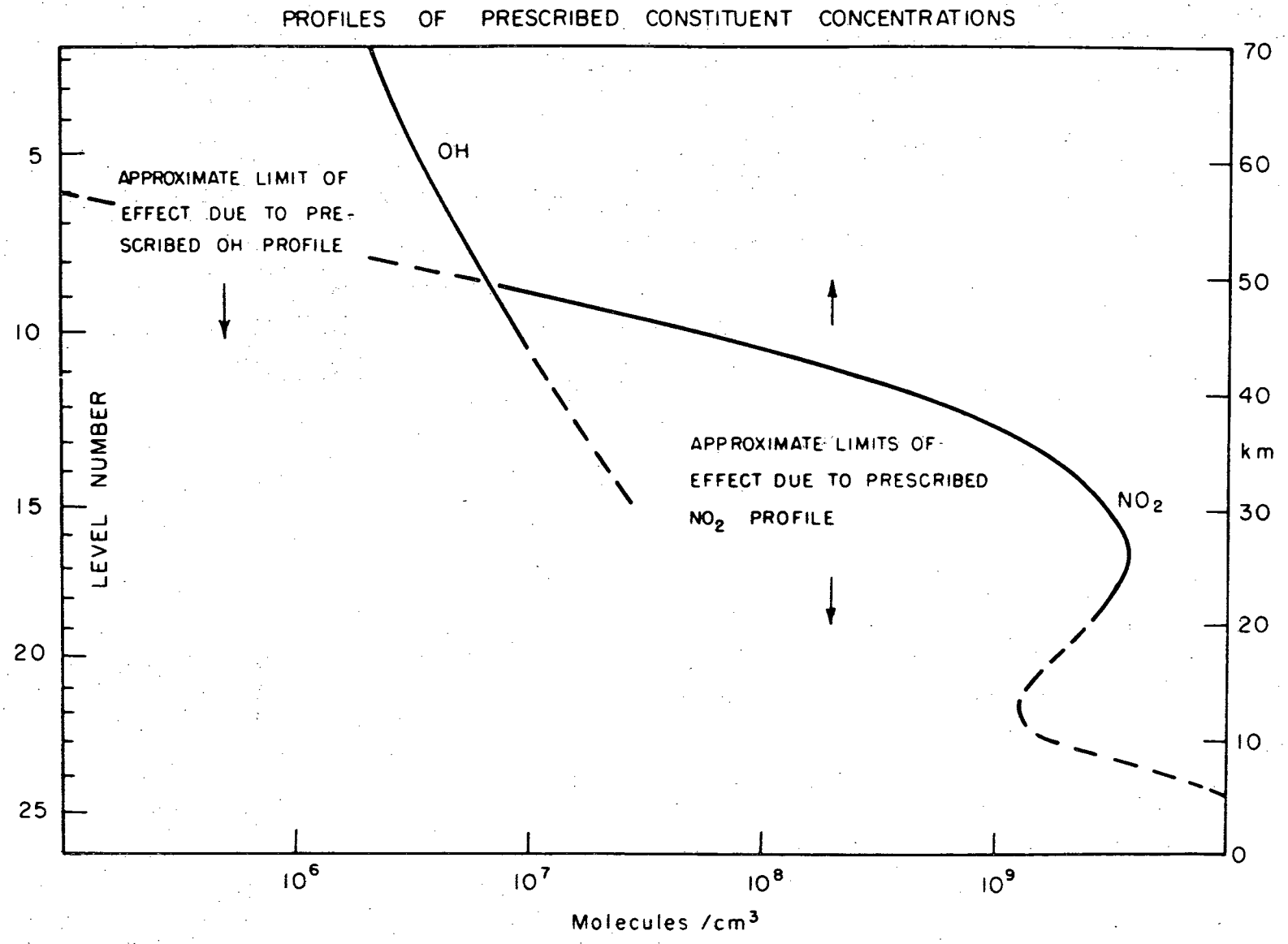
PROFILES OF PRESCRIBED CONSTITUENT CONCENTRATIONS
OH
APPROXIMATE LIMIT OF EFFECT DUE TO PRESCRIBED OH PROFILE
APPROXIMATE LIMITS OF EFFECT DUE TO PRESCRIBED NO2 PROFILE
NO2
LEVEL NUMBER
5
10
15
20
25
70
60
50
40
30
20
10
0
km
10^6
10^7
10^8
10^9
Molecules /cm^3

Fig. 6.

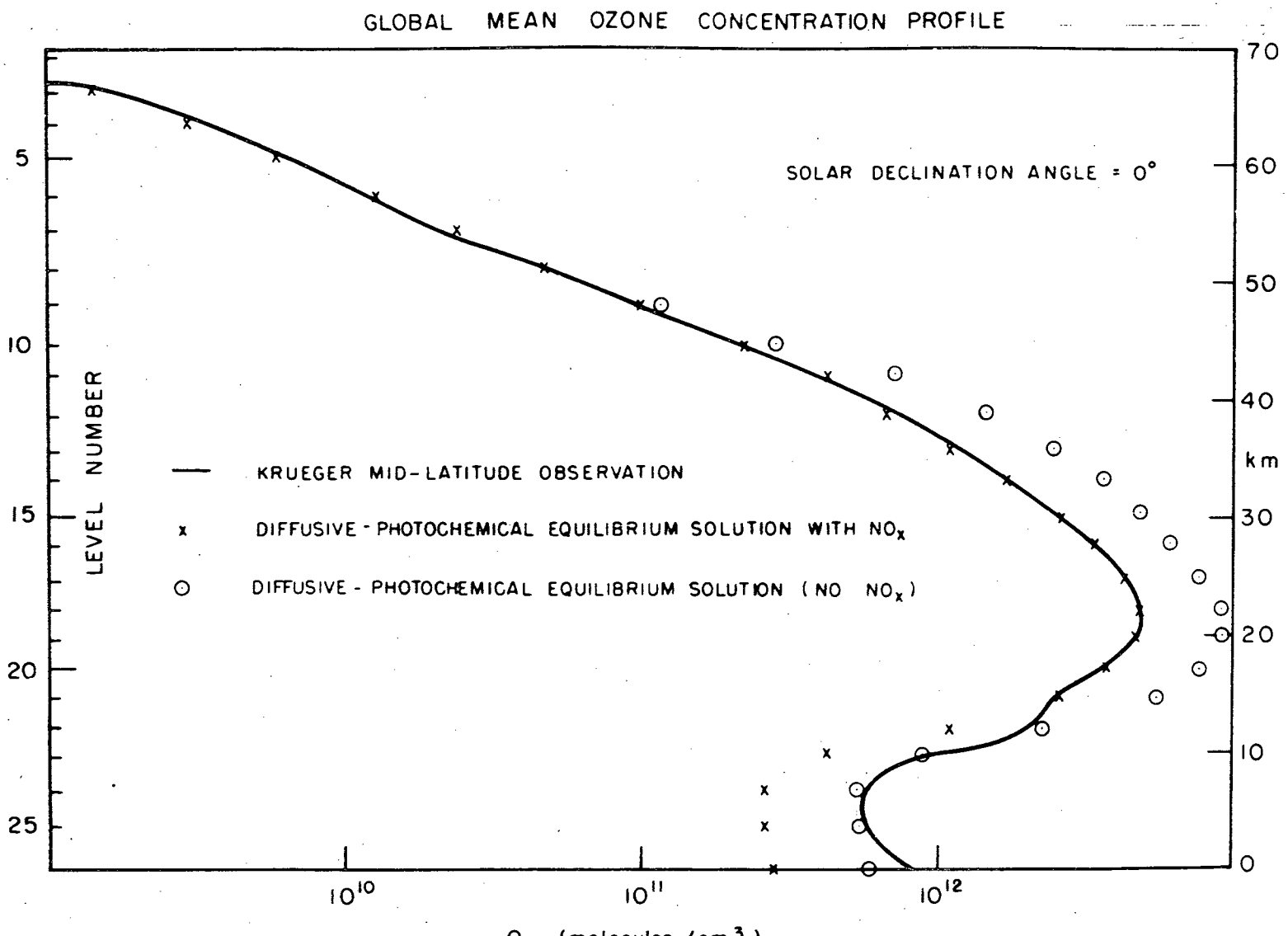
GLOBAL MEAN OZONE CONCENTRATION PROFILE
SOLAR DECLINATION ANGLE = 0°
KRUEGER MID-LATITUDE OBSERVATION
DIFFUSIVE - PHOTOCHEMICAL EQUILIBRIUM SOLUTION WITH NO_x
DIFFUSIVE - PHOTOCHEMICAL EQUILIBRIUM SOLUTION (NO NO_x)
LEVEL NUMBER
5
10
15
20
25
70
60
50
40
30
20
10
0
km
10^{10}
10^{11}
10^{12}
O_3 (molecules /cm^3)

Fig. 7.

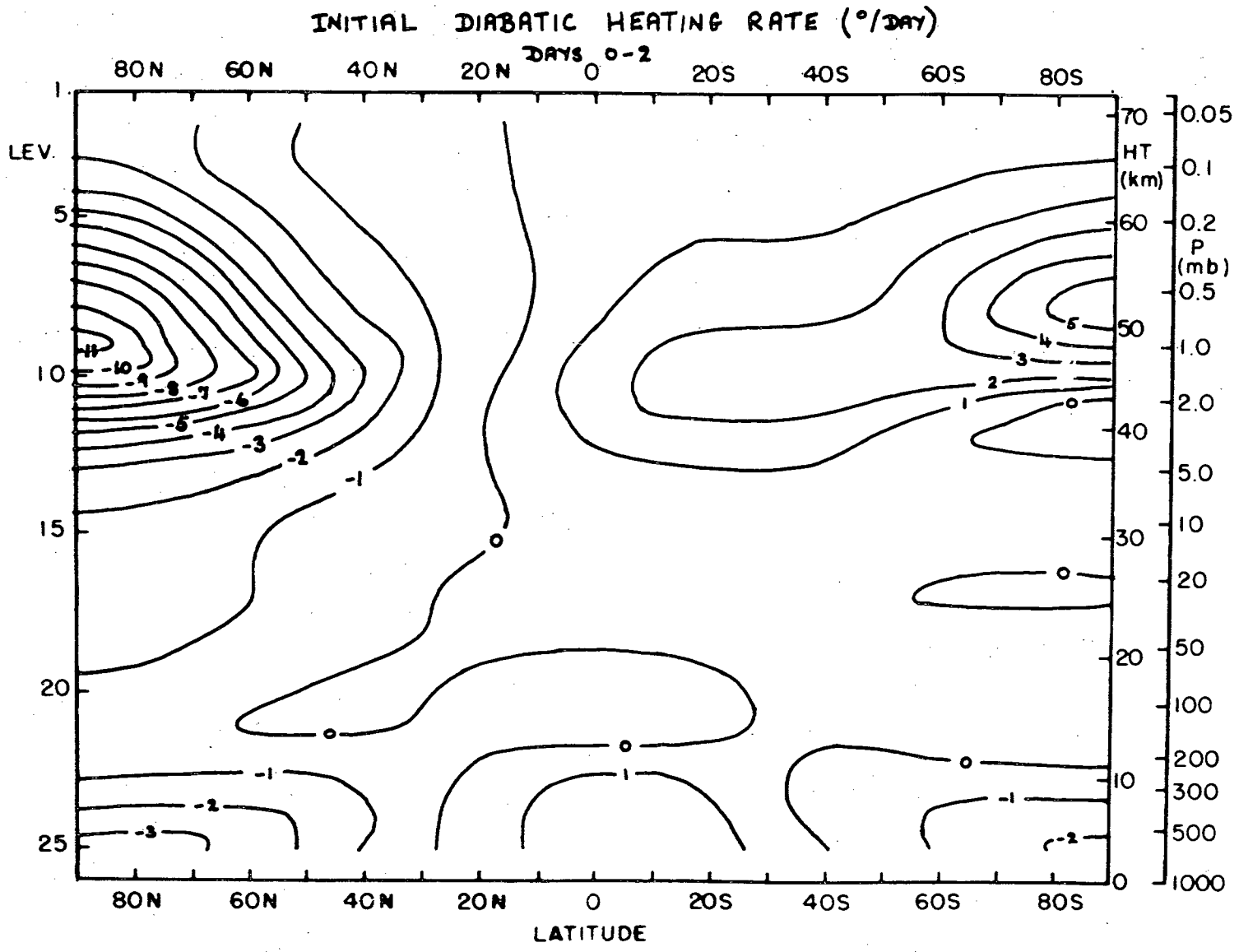
INITIAL DIABATIC HEATING RATE (°/DAY)
DAYS 0-2
80N
60N
40N
20N
0
20S
40S
60S
80S
LEV.
1
5
10
15
20
25
HT (km)
70
60
50
40
30
20
10
0
P (mb)
0.05
0.1
0.2
0.5
1.0
2.0
5.0
10
20
50
100
200
300
500
1000
LATITUDE

Fig. 8.

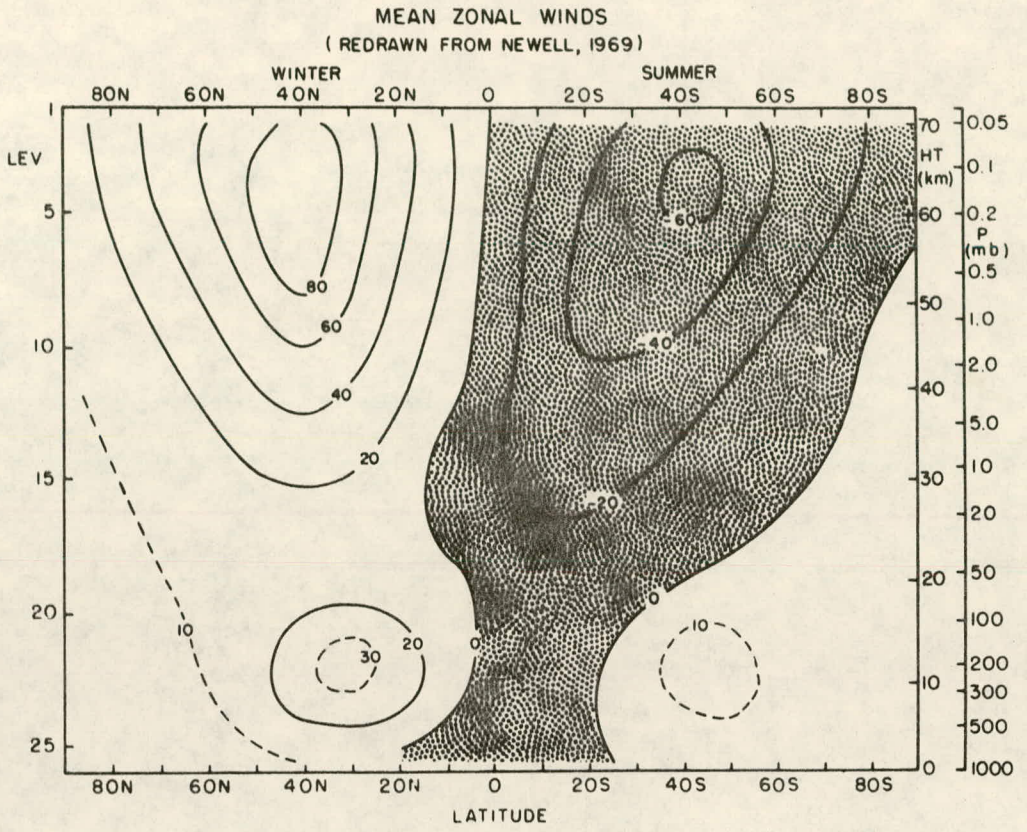
MEAN ZONAL WINDS
(REDRAWN FROM NEWELL, 1969)
WINTER
SUMMER
80N 60N 40N 20N 0 20S 40S 60S 80S
LEV
HT (km)
P (mb)
LATITUDE

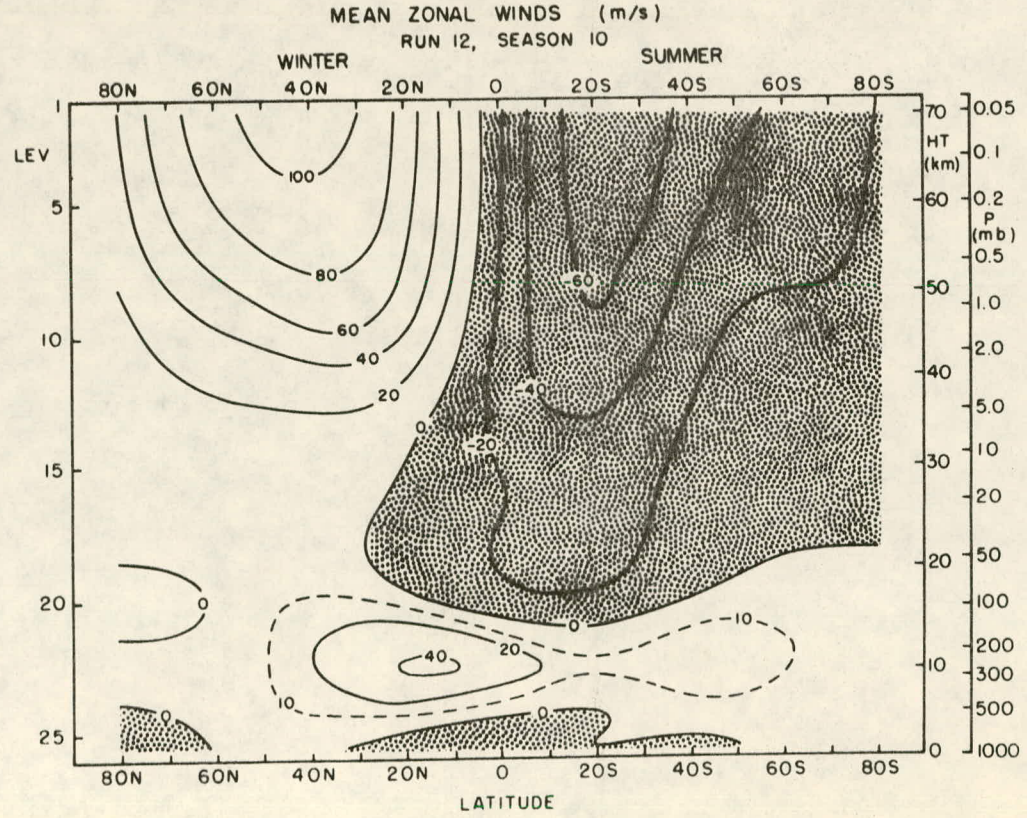
MEAN ZONAL WINDS (m/s)
RUN 12, SEASON 10
WINTER
SUMMER
80N 60N 40N 20N 0 20S 40S 60S 80S
LEV
HT (km)
P (mb)
LATITUDE

Fig. 9.

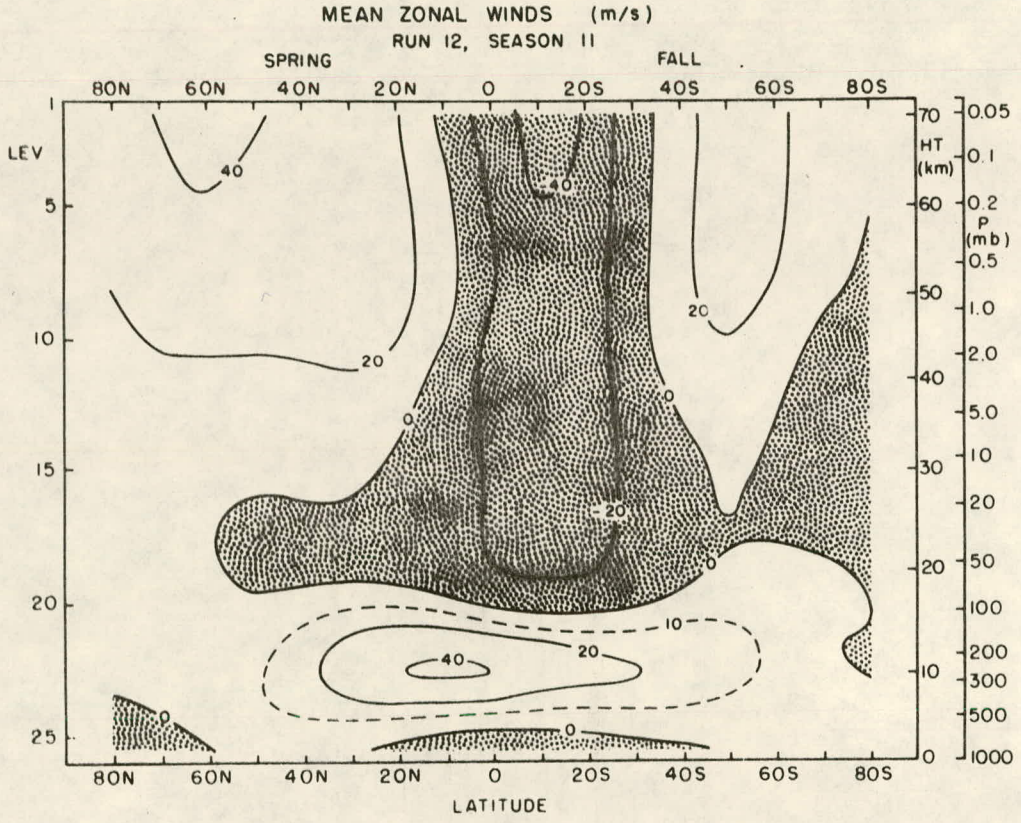
MEAN ZONAL WINDS (m/s)
RUN 12, SEASON 11
SPRING
FALL
80N
60N
40N
20N
0
20S
40S
60S
80S
LEV
1
5
10
15
20
25
HT (km)
70
60
50
40
30
20
10
0
P (mb)
0.05
0.1
0.2
0.5
1.0
2.0
5.0
10
20
50
100
200
300
500
1000
40
20
0
-20
10
LATITUDE

Fig. 10.

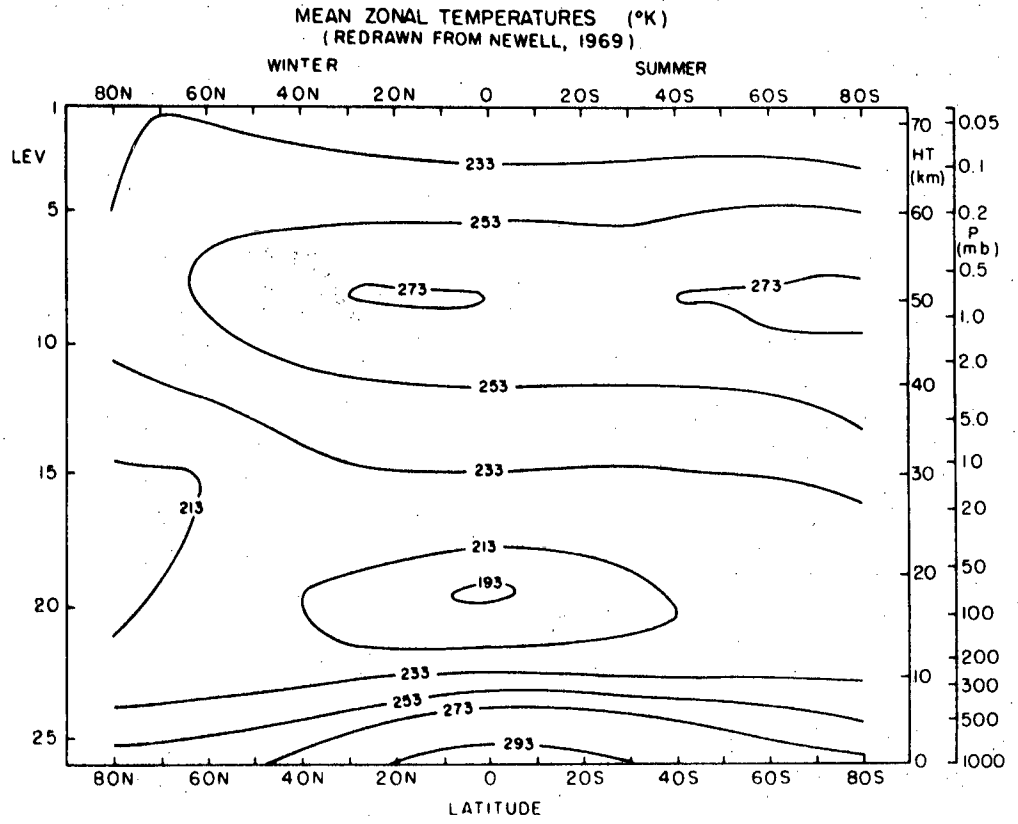
MEAN ZONAL TEMPERATURES (°K)
(REDRAWN FROM NEWELL, 1969)
WINTER
SUMMER
80N 60N 40N 20N 0 20S 40S 60S 80S
LEV
HT (km)
P (mb)
233
253
273
213
193
293
LATITUDE

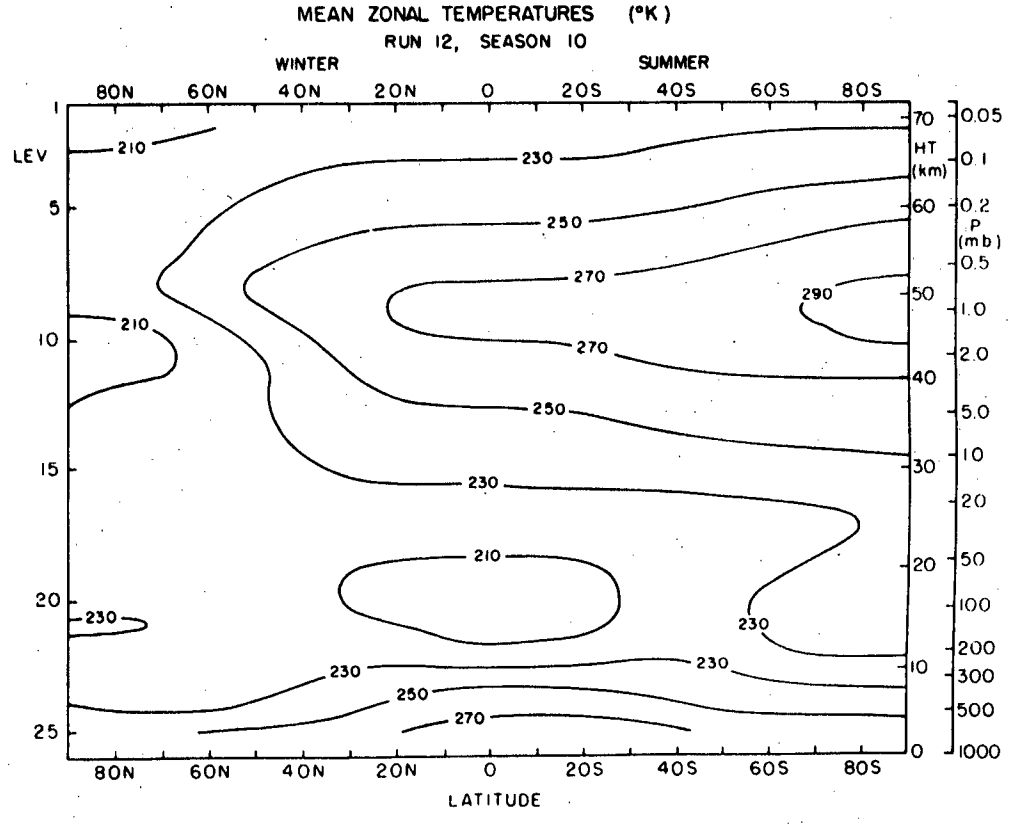
MEAN ZONAL TEMPERATURES (°K)
RUN 12, SEASON 10
WINTER
SUMMER
80N 60N 40N 20N 0 20S 40S 60S 80S
LEV
HT (km)
P (mb)
210
230
250
270
290
LATITUDE

Fig. 11.

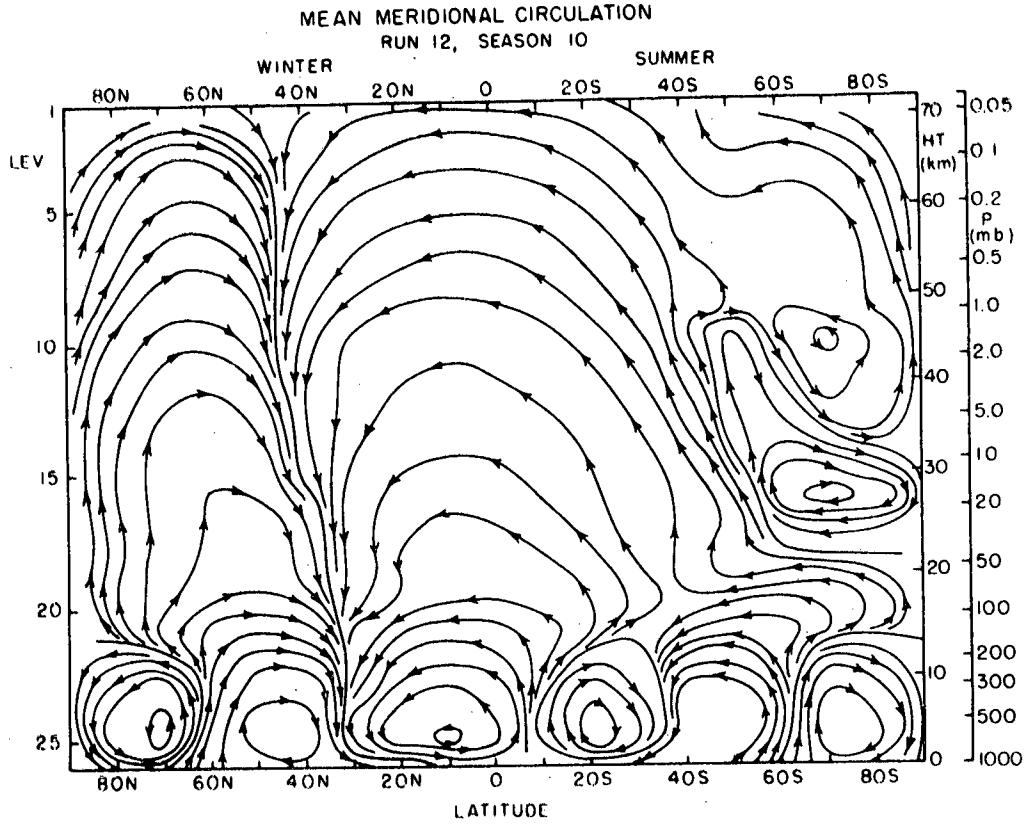
MEAN MERIDIONAL CIRCULATION
RUN 12, SEASON 10
WINTER
SUMMER
80N 60N 40N 20N 0 20S 40S 60S 80S
LEV
HT (km)
P (mb)
LATITUDE

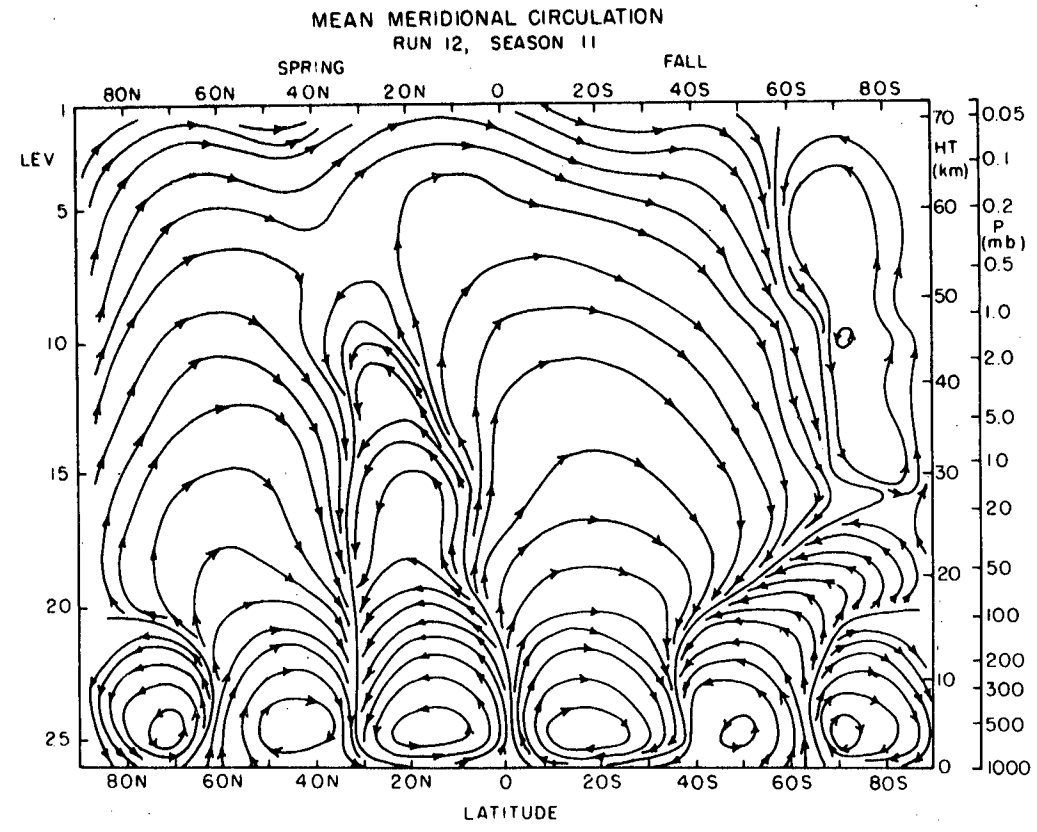
MEAN MERIDIONAL CIRCULATION
RUN 12, SEASON 11
SPRING
FALL
80N 60N 40N 20N 0 20S 40S 60S 80S
LEV
HT (km)
P (mb)
LATITUDE

Fig. 12.

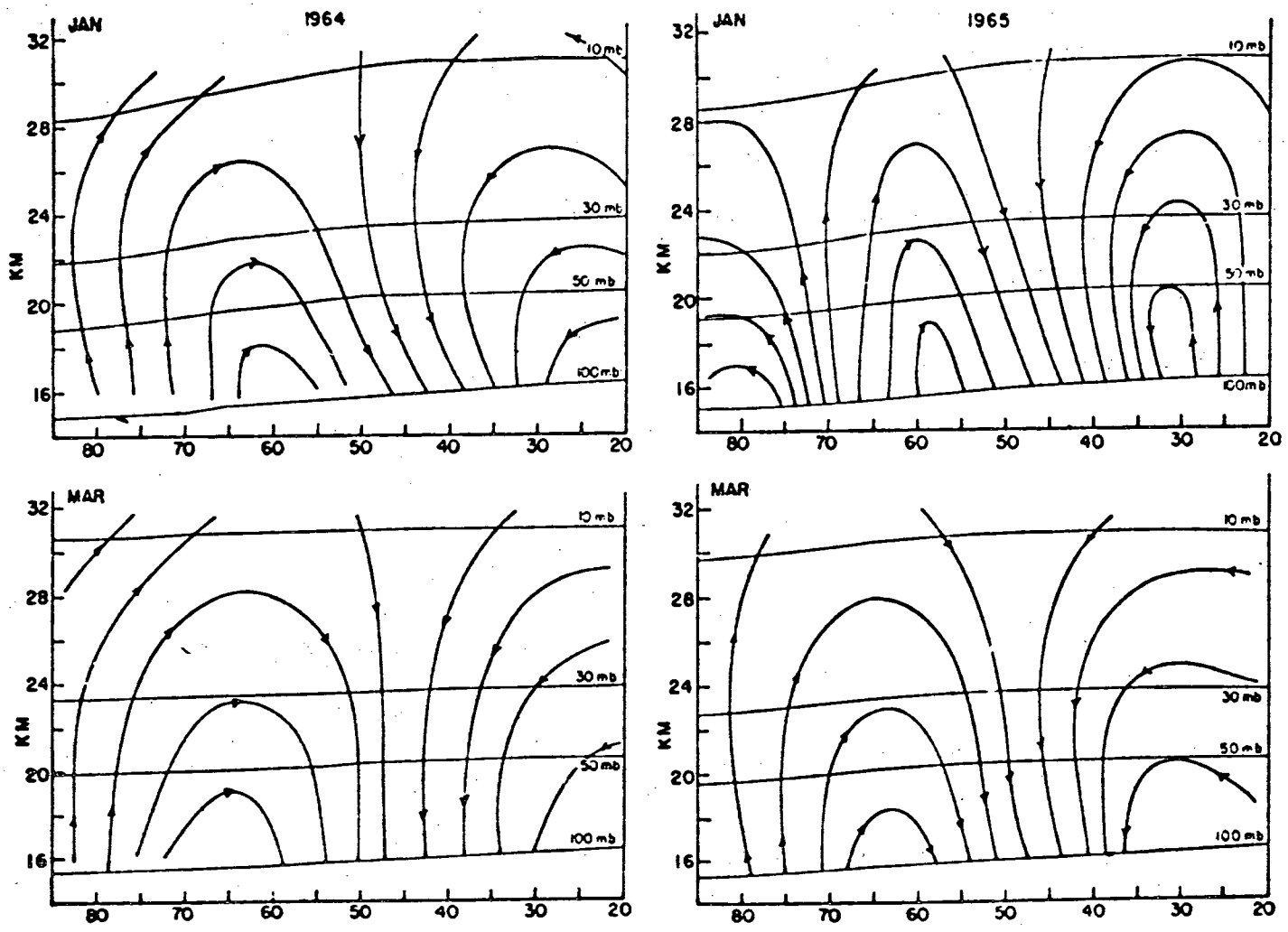
JAN
1964
10 mb
30 mb
50 mb
100 mb
KM
32
28
24
20
16
80
70
60
50
40
30
20
JAN
1965
10 mb
30 mb
50 mb
100 mb
MAR
10 mb
30 mb
50 mb
100 mb
MAR
10 mb
30 mb
50 mb
100 mb

Fig. 13.

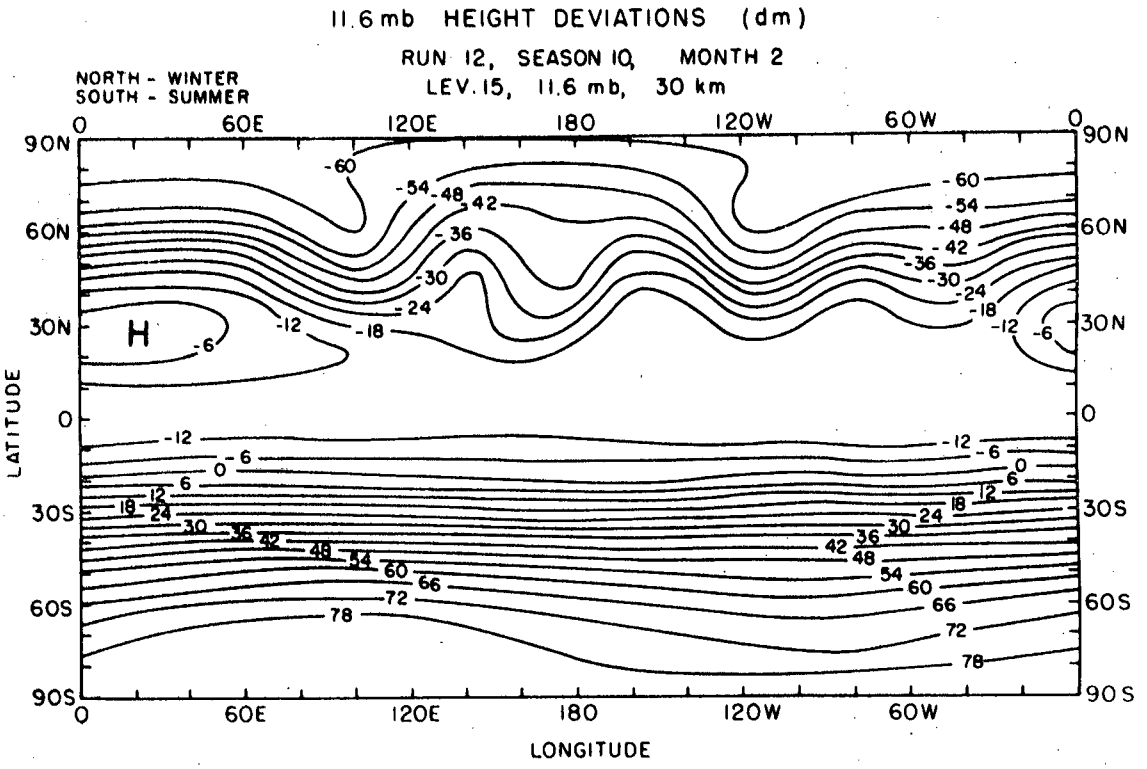
11.6 mb HEIGHT DEVIATIONS (dm)
RUN 12, SEASON 10, MONTH 2
LEV. 15, 11.6 mb, 30 km
NORTH - WINTER
SOUTH - SUMMER
LATITUDE
LONGITUDE
90N
60N
30N
0
30S
60S
90S
0
60E
120E
180
120W
60W
H
-60
-54
-48
-42
-36
-30
-24
-18
-12
-6
0
6
12
18
24
30
36
42
48
54
60
66
72
78

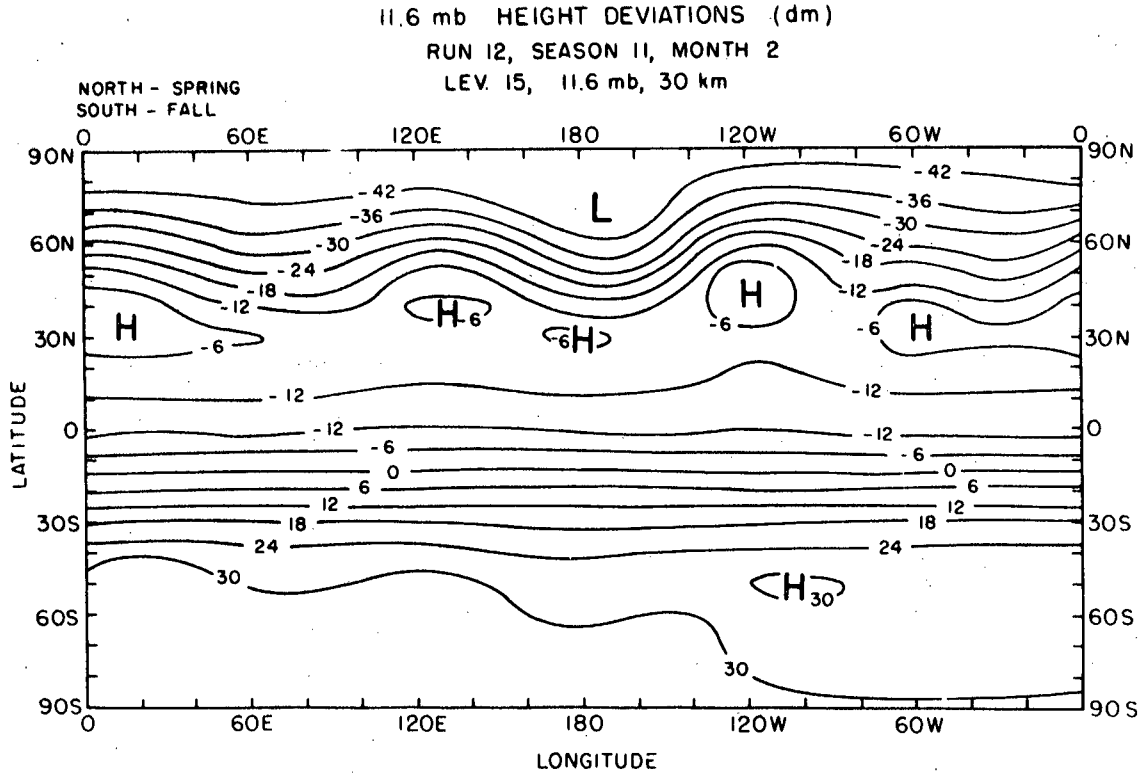
11.6 mb HEIGHT DEVIATIONS (dm)
RUN 12, SEASON 11, MONTH 2
LEV. 15, 11.6 mb, 30 km
NORTH - SPRING
SOUTH - FALL
LATITUDE
LONGITUDE
90N
60N
30N
0
30S
60S
90S
0
60E
120E
180
120W
60W
L
H
H6
6H
-42
-36
-30
-24
-18
-12
-6
0
6
12
18
24
30

Fig. 14.

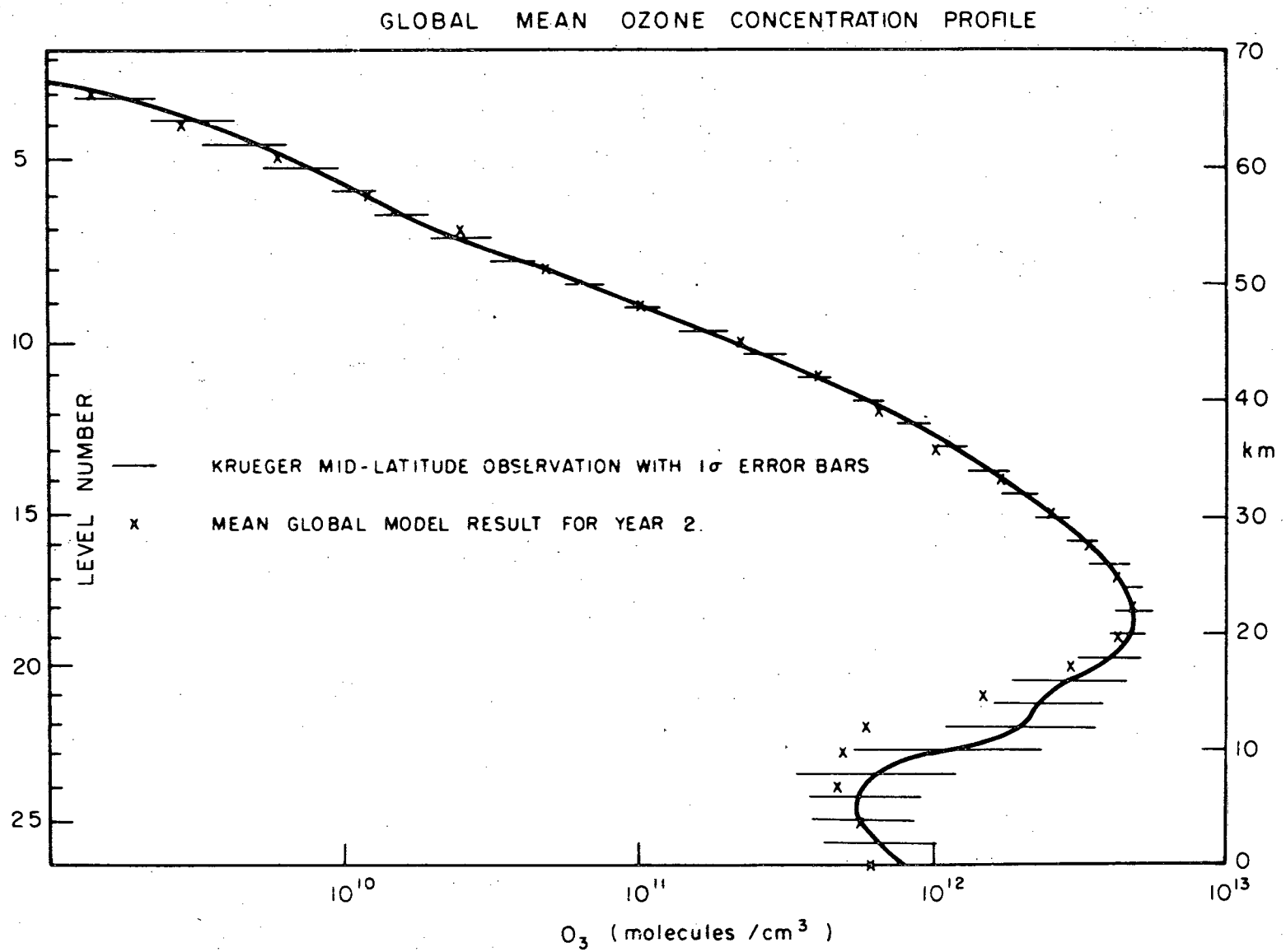
GLOBAL MEAN OZONE CONCENTRATION PROFILE
LEVEL NUMBER
5
10
15
20
25
70
60
50
40
30
20
10
0
km
KRUEGER MID-LATITUDE OBSERVATION WITH 1σ ERROR BARS
MEAN GLOBAL MODEL RESULT FOR YEAR 2.
10^{10}
10^{11}
10^{12}
10^{13}
O_3 (molecules /cm^3)

Fig. 15.

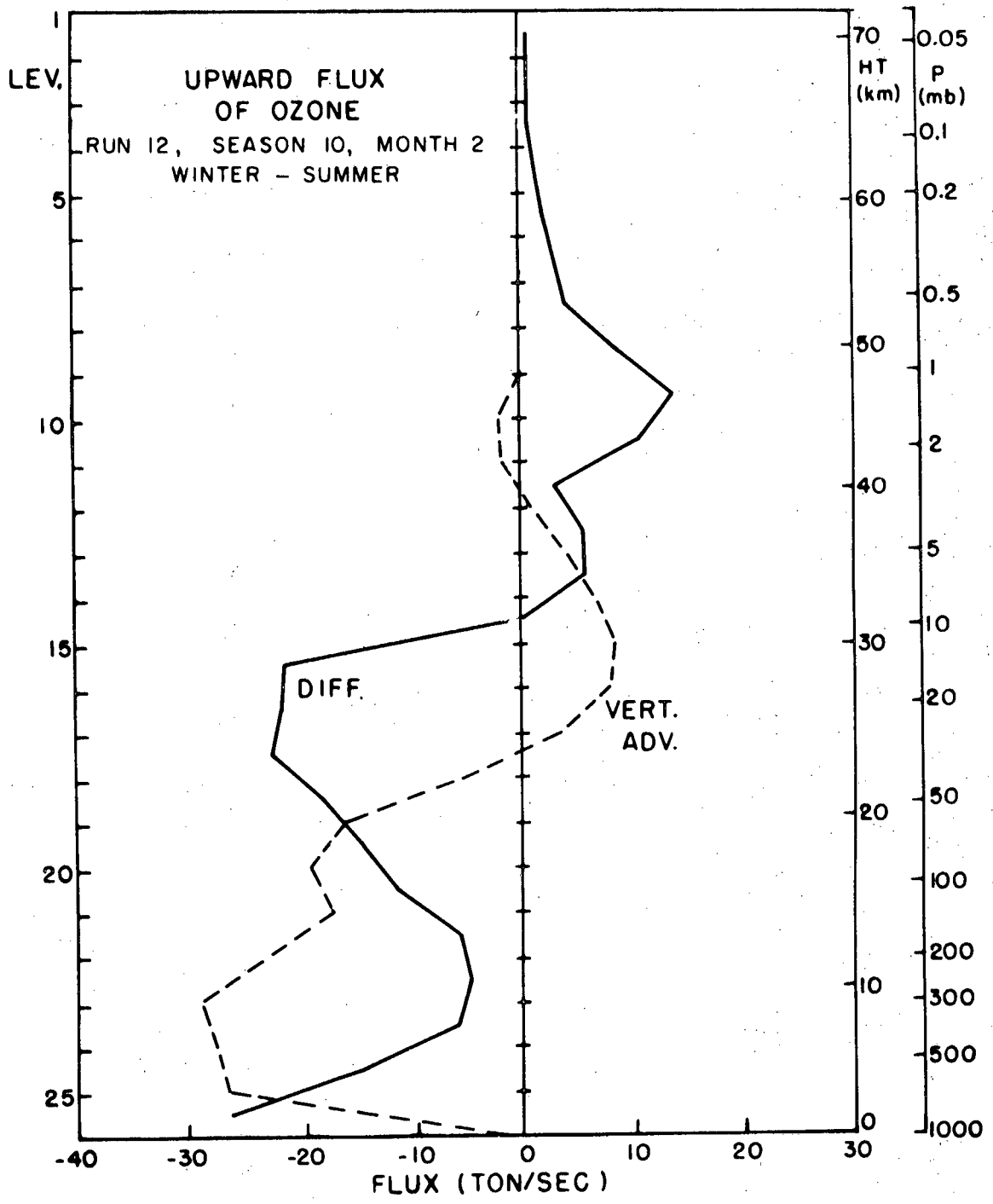
UPWARD FLUX
OF OZONE
RUN 12, SEASON 10, MONTH 2
WINTER – SUMMER
LEV.
HT (km)
P (mb)
DIFF.
VERT. ADV.
FLUX (TON/SEC)
1
5
10
15
20
25
70
60
50
40
30
20
10
0
0.05
0.1
0.2
0.5
1
2
5
10
20
50
100
200
300
500
1000
-40
-30
-20
-10
0
10
20
30

Fig. 16.

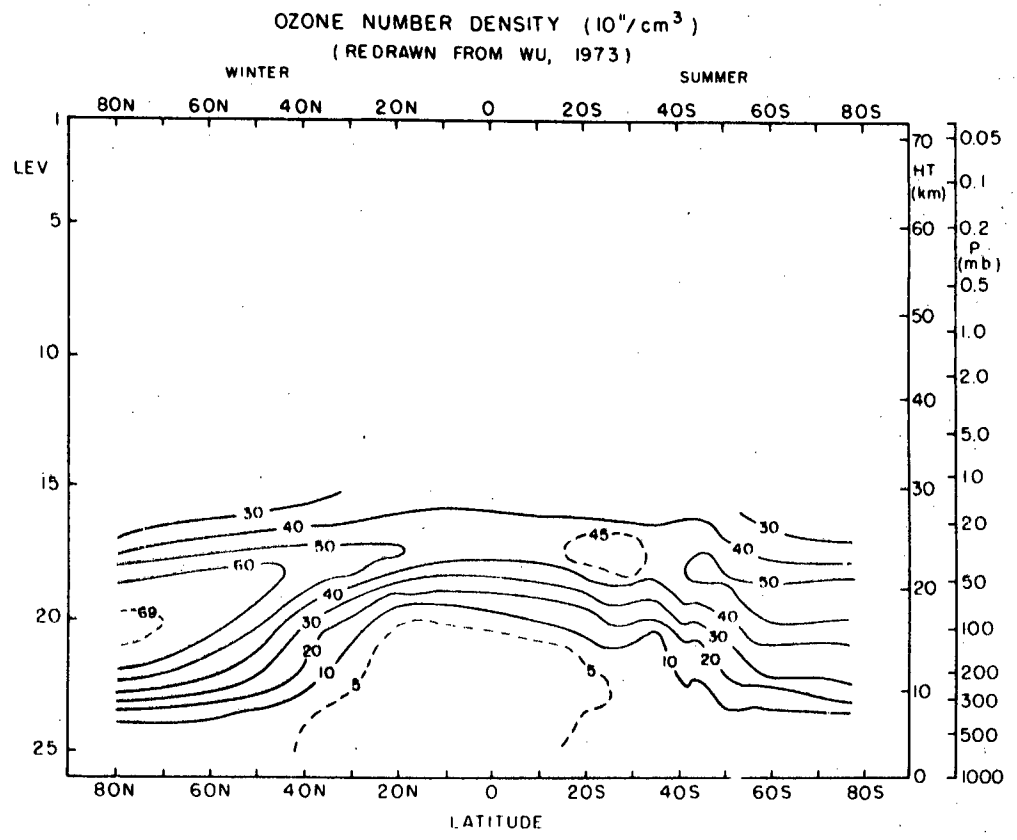
OZONE NUMBER DENSITY (10"/cm³)
(REDRAWN FROM WU, 1973)
WINTER
SUMMER
80N 60N 40N 20N 0 20S 40S 60S 80S
LEV
HT (km)
P (mb)
LATITUDE

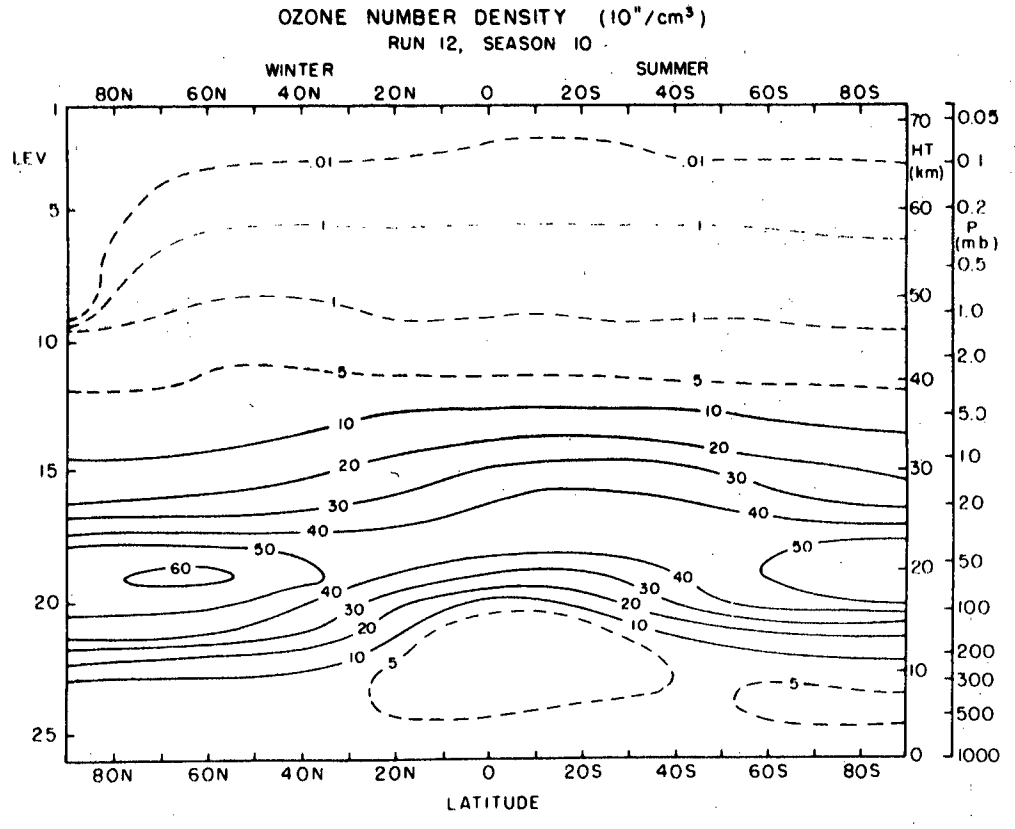
OZONE NUMBER DENSITY (10"/cm³)
RUN 12, SEASON 10
WINTER
SUMMER
80N 60N 40N 20N 0 20S 40S 60S 80S
LEV
HT (km)
P (mb)
LATITUDE

Fig. 17.

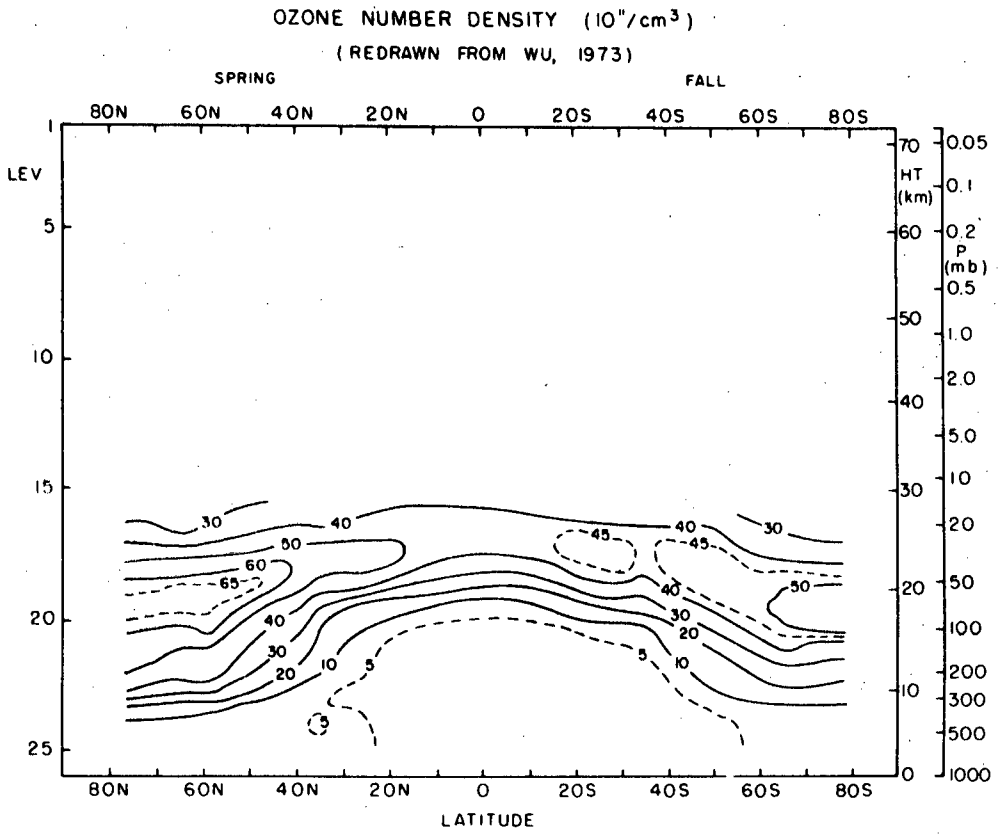
OZONE NUMBER DENSITY (10"/cm³)
(REDRAWN FROM WU, 1973)
SPRING
FALL
80N 60N 40N 20N 0 20S 40S 60S 80S
LEV
HT (km)
P (mb)
LATITUDE

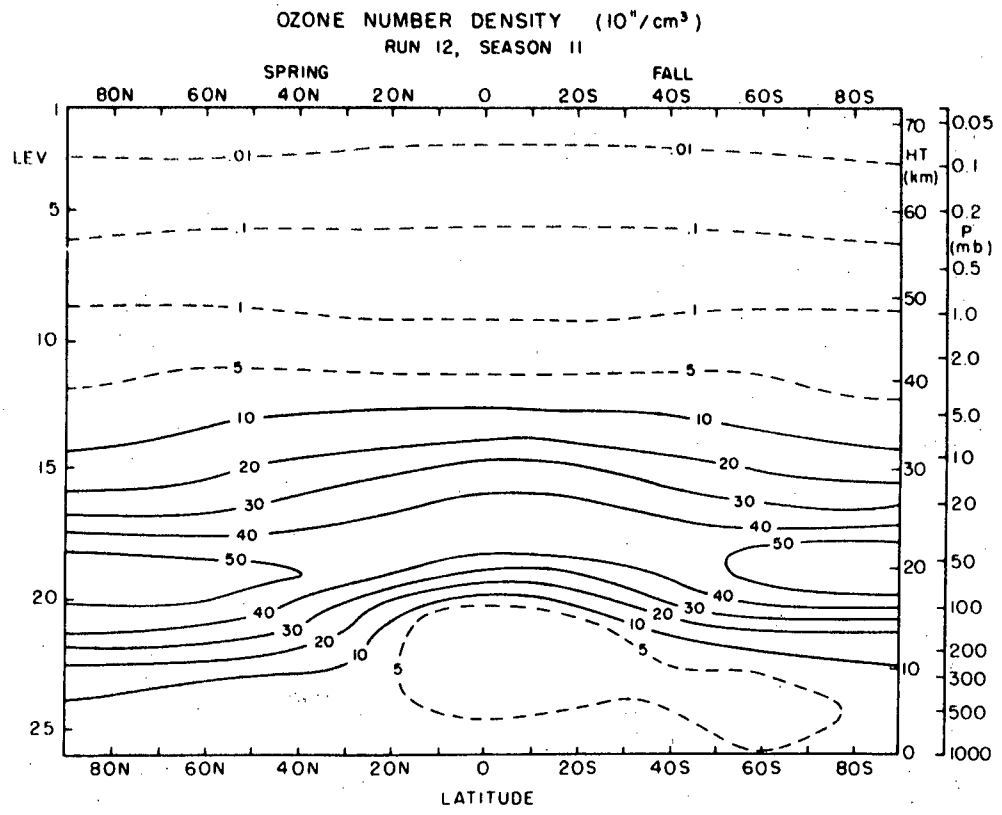
OZONE NUMBER DENSITY (10"/cm³)
RUN 12, SEASON 11
SPRING
FALL
80N 60N 40N 20N 0 20S 40S 60S 80S
LEV
HT (km)
P (mb)
LATITUDE

Fig. 18.

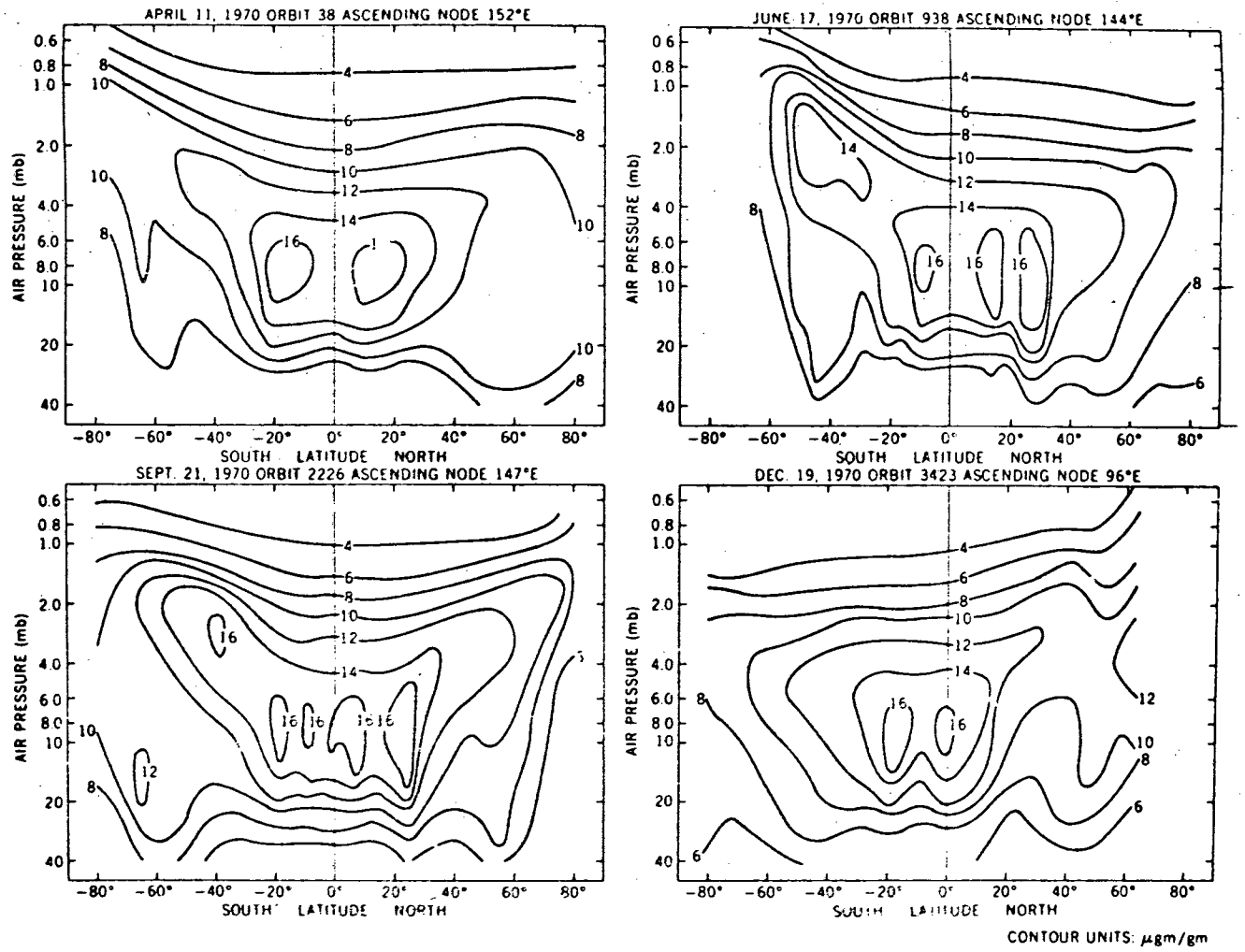
APRIL 11, 1970 ORBIT 38 ASCENDING NODE 152°E
JUNE 17, 1970 ORBIT 938 ASCENDING NODE 144°E
SEPT. 21, 1970 ORBIT 2226 ASCENDING NODE 147°E
DEC. 19, 1970 ORBIT 3423 ASCENDING NODE 96°E
AIR PRESSURE (mb)
0.6
0.8
1.0
2.0
4.0
6.0
8.0
10
20
40
-80° -60° -40° -20° 0° 20° 40° 60° 80°
SOUTH LATITUDE NORTH
CONTOUR UNITS: μgm/gm

Fig. 19.

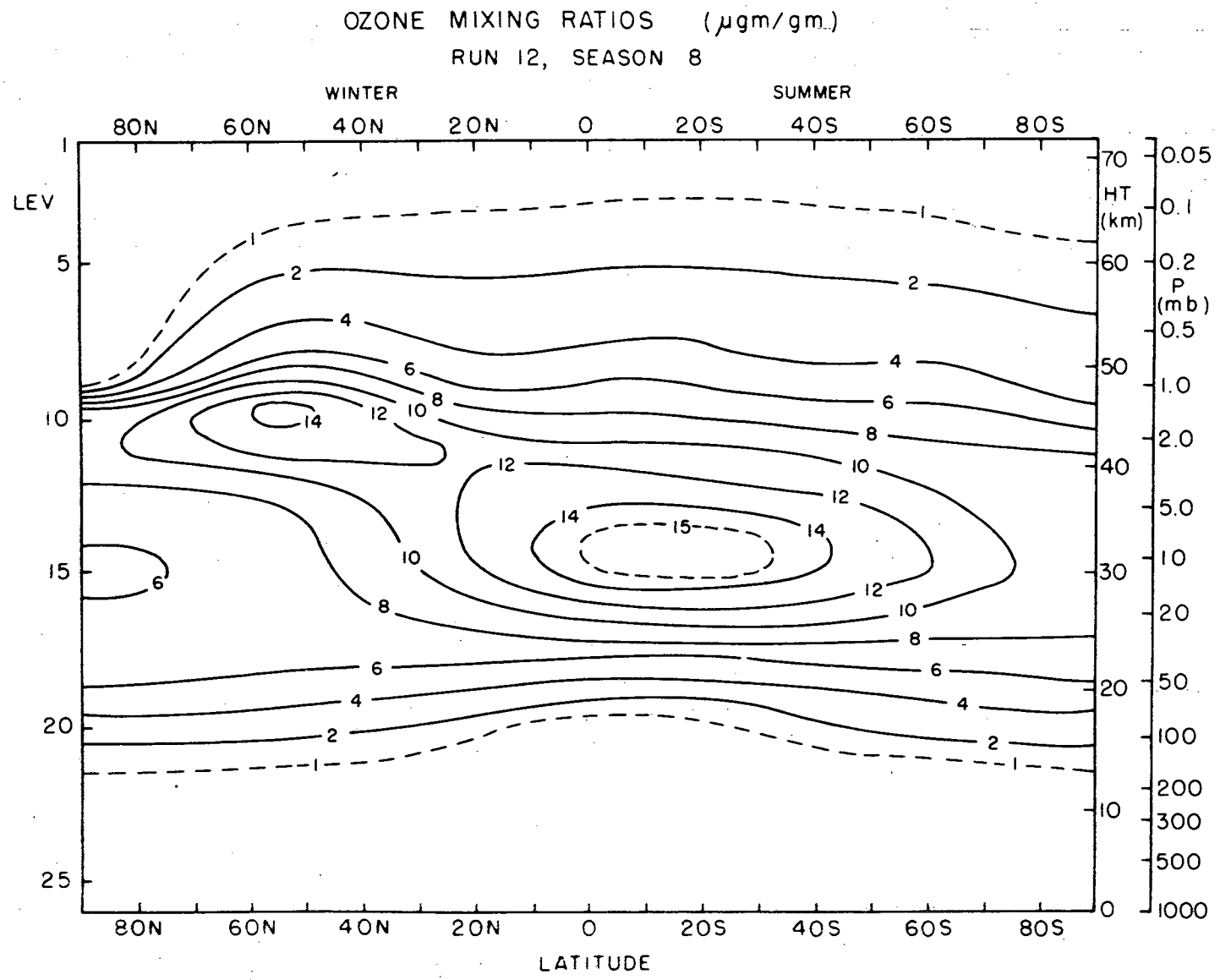
OZONE MIXING RATIOS (μgm/gm)
RUN 12, SEASON 8
WINTER
SUMMER
80N
60N
40N
20N
0
20S
40S
60S
80S
LEV
HT (km)
P (mb)
LATITUDE

Fig. 20.

TOTAL OZONE (10^{-3} cm) AS A FUNCTION OF SEASON AND LATITUDE

REDRAWN FROM DÜTSCH, 1969

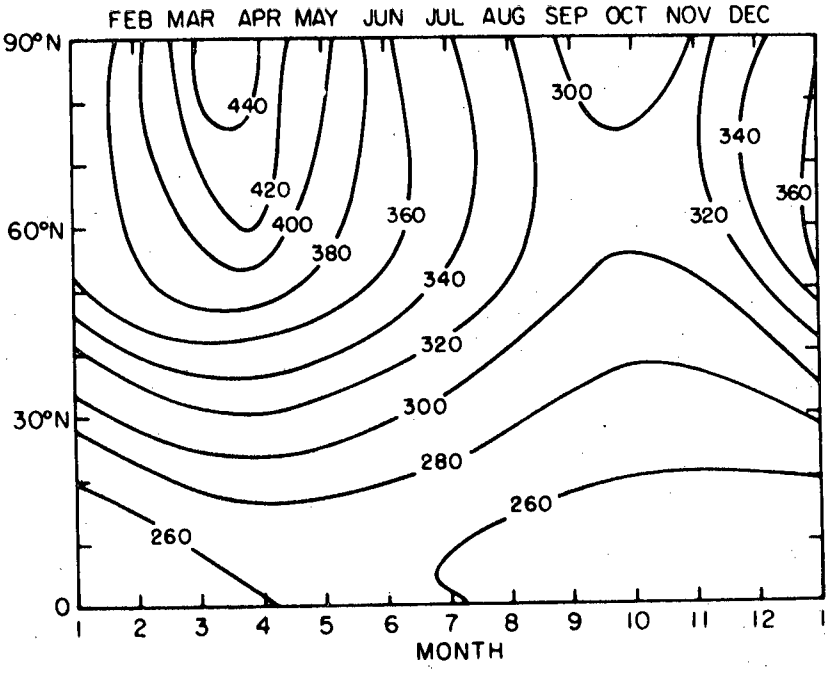

RUN 12 MEAN USING SEASONS 5 - 10

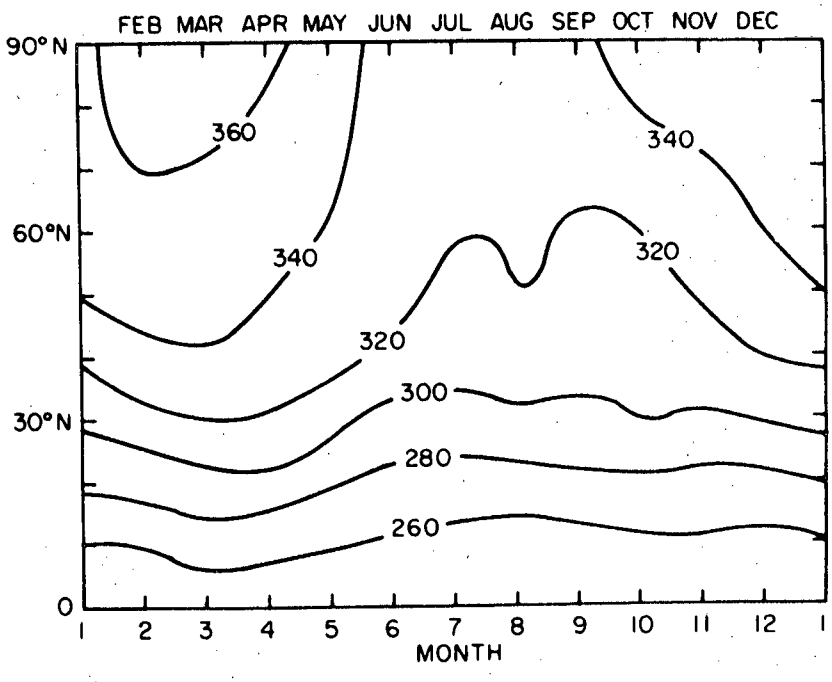

Fig. 21.

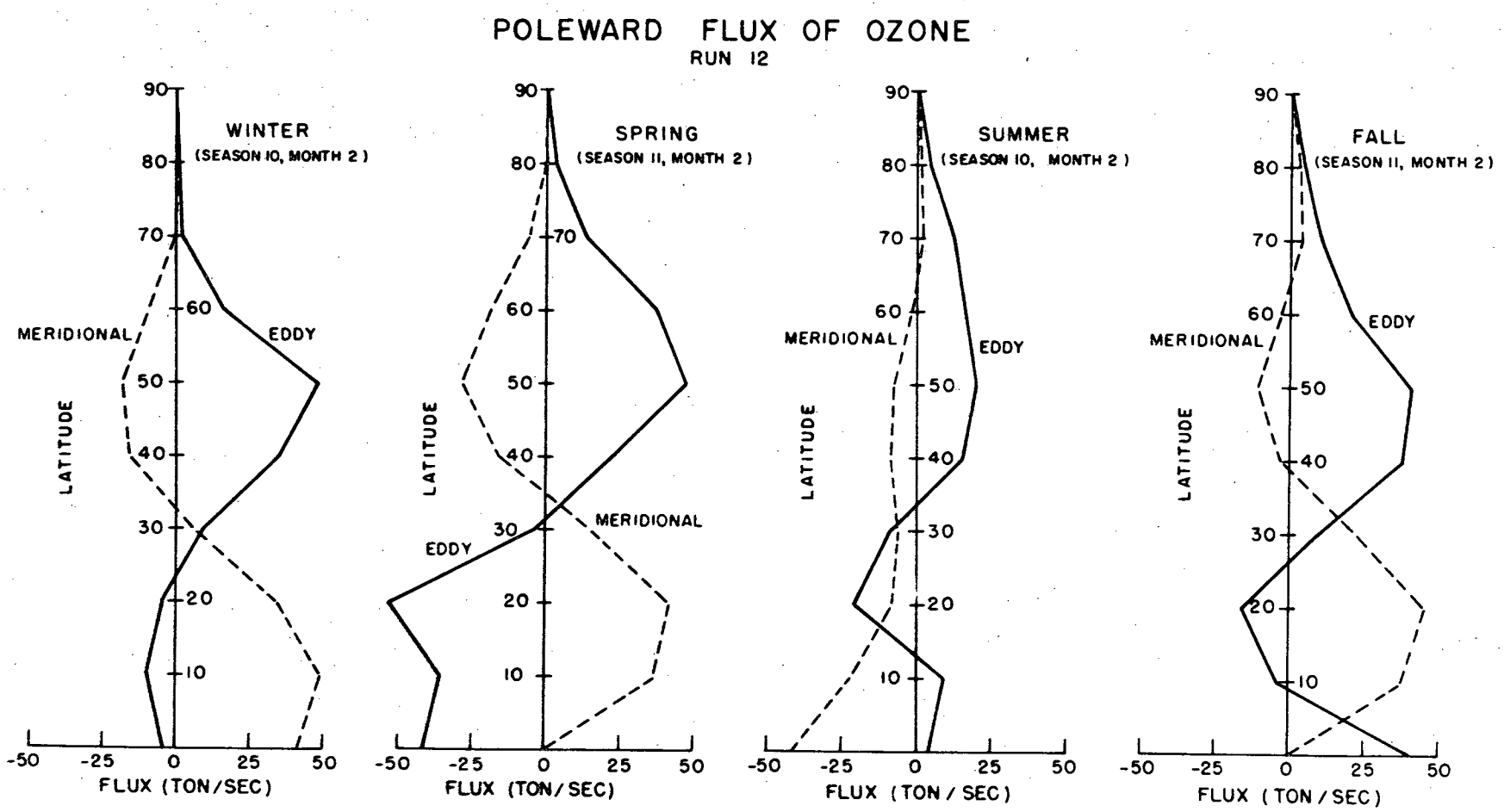
POLEWARD FLUX OF OZONE
RUN 12
WINTER
(SEASON 10, MONTH 2)
SPRING
(SEASON 11, MONTH 2)
SUMMER
(SEASON 10, MONTH 2)
FALL
(SEASON 11, MONTH 2)
MERIDIONAL
EDDY
LATITUDE
FLUX (TON/SEC)
90
80
70
60
50
40
30
20
10
-50
-25
0
25
50

Fig. 22.

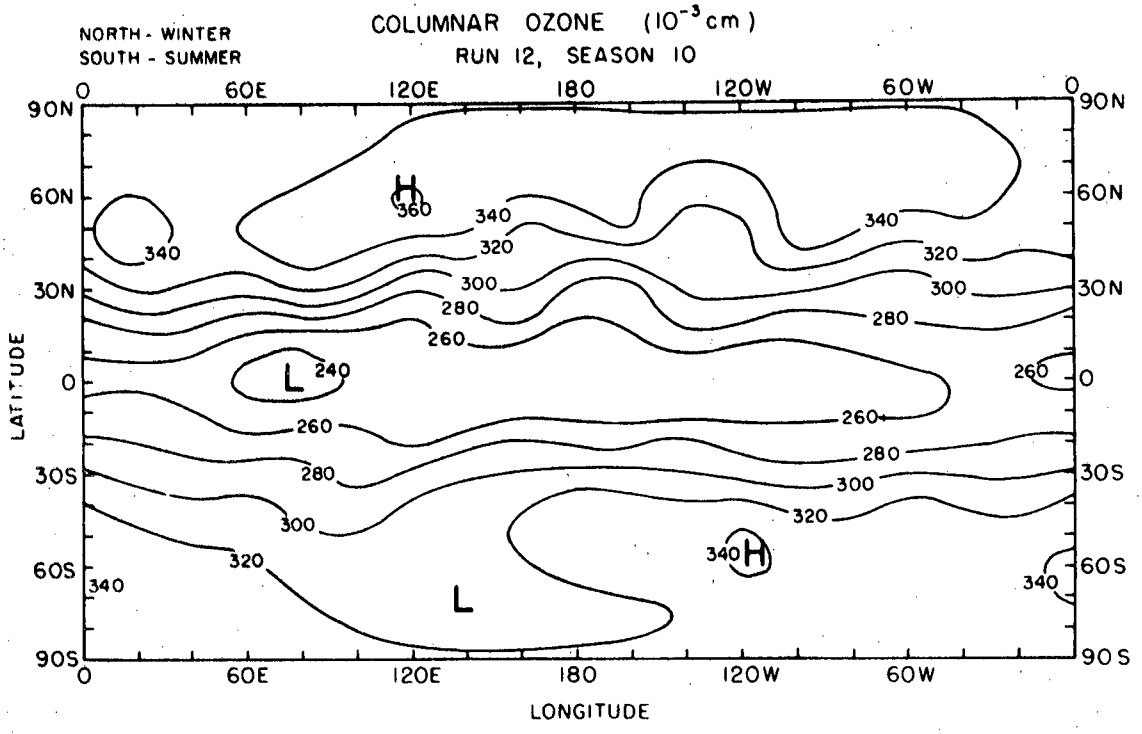
NORTH - WINTER
SOUTH - SUMMER
COLUMNAR OZONE (10⁻³cm)
RUN 12, SEASON 10
0
60E
120E
180
120W
60W
90N
60N
30N
0
30S
60S
90S
LATITUDE
LONGITUDE
H
360
340
320
300
280
260
L
240

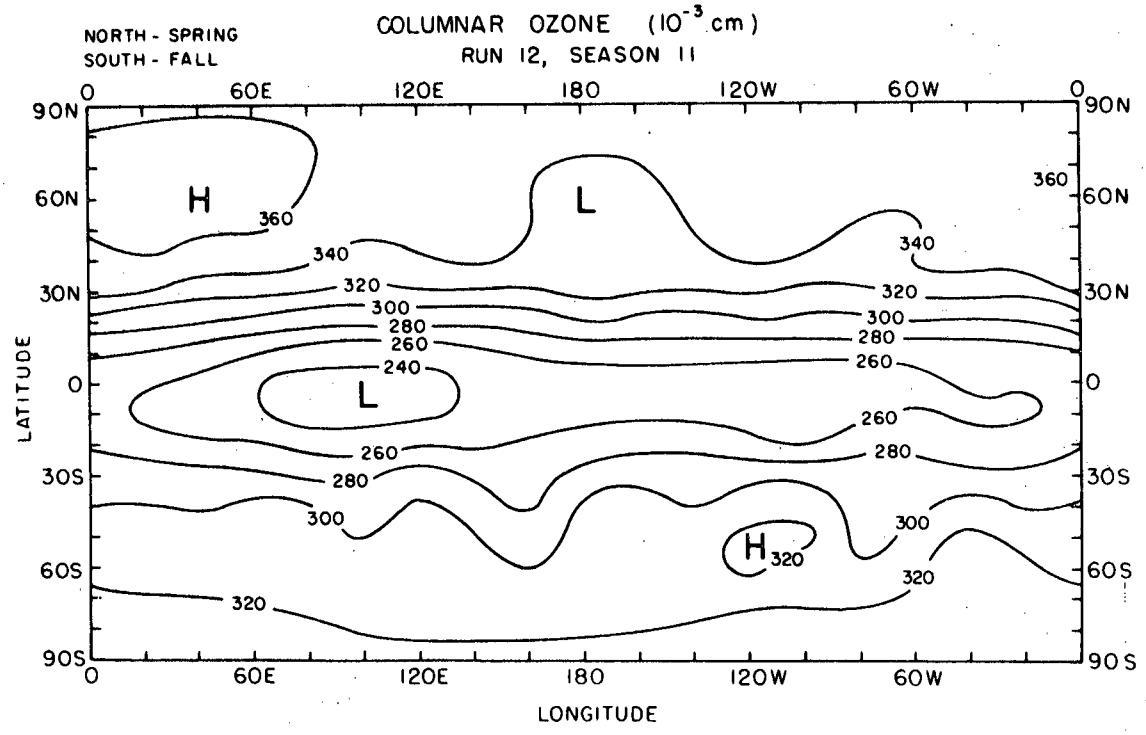
NORTH - SPRING
SOUTH - FALL
COLUMNAR OZONE (10⁻³cm)
RUN 12, SEASON 11
0
60E
120E
180
120W
60W
90N
60N
30N
0
30S
60S
90S
LATITUDE
LONGITUDE
H
360
L
340
320
300
280
260
240
H
320

Fig. 23.

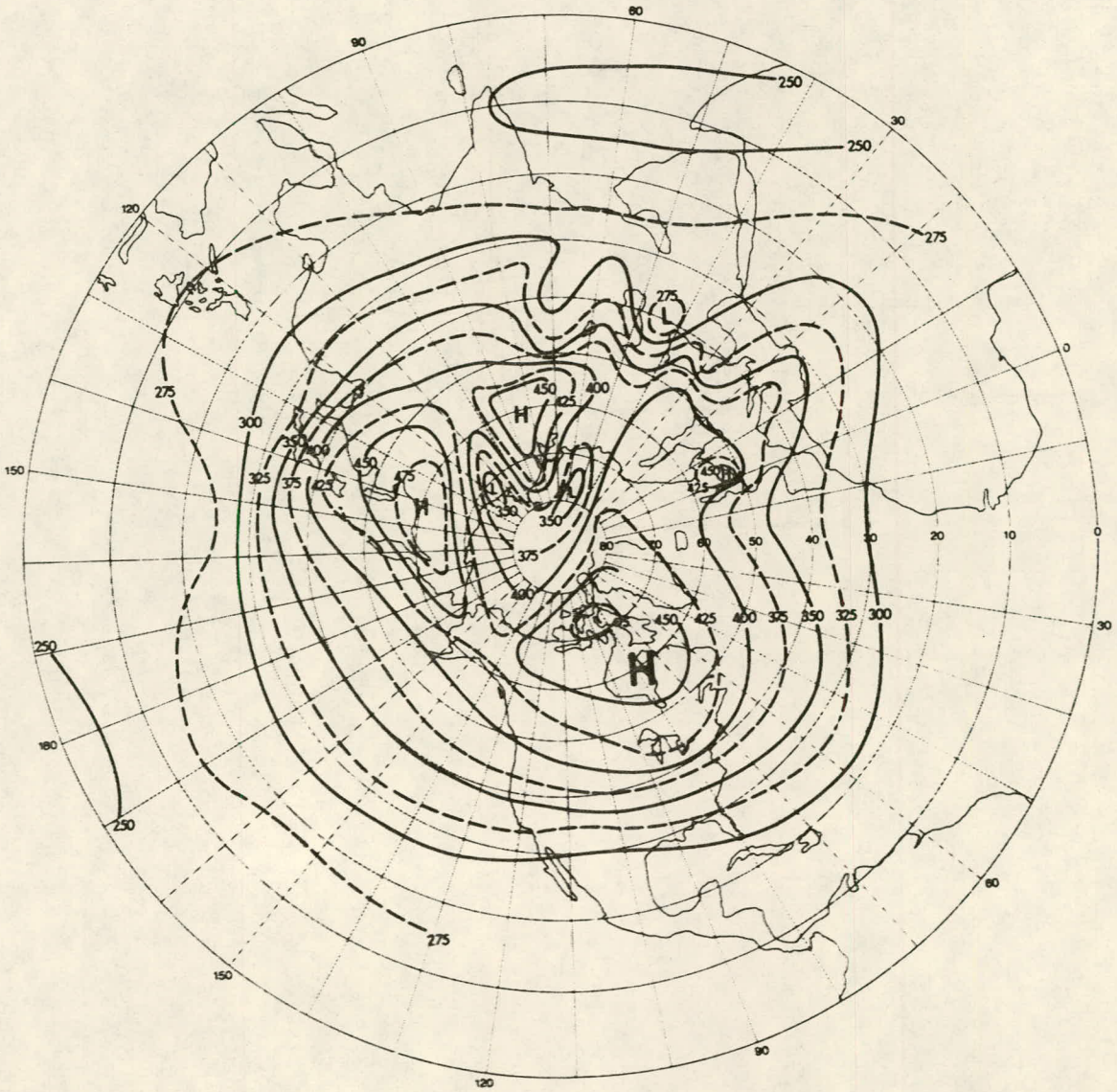
80
90
120
150
180
250
275
300
325
350
375
400
425
450
H
L
D
0
10
20
30
40
50
60

Fig. 24a.

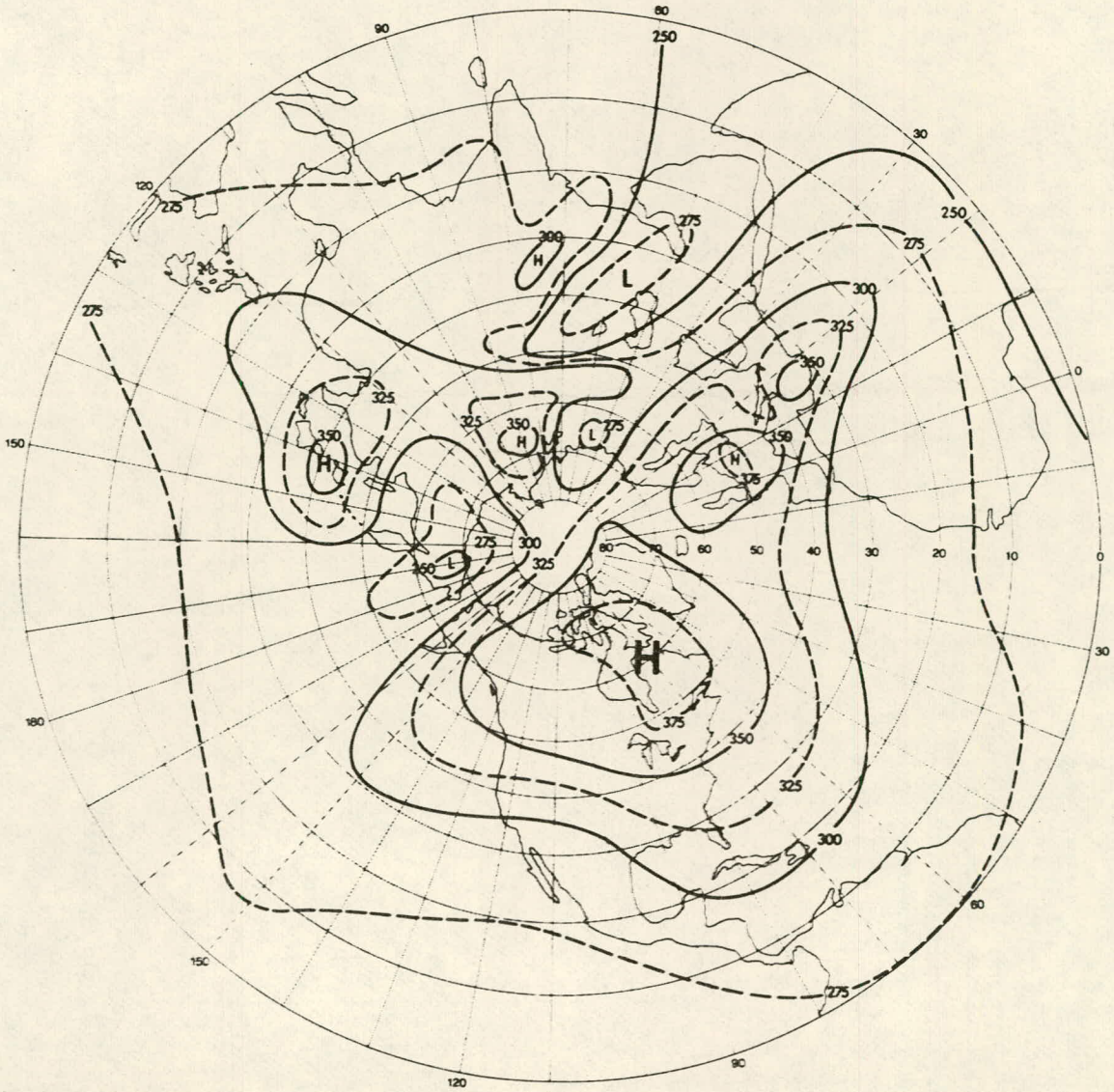

Fig. 24b.

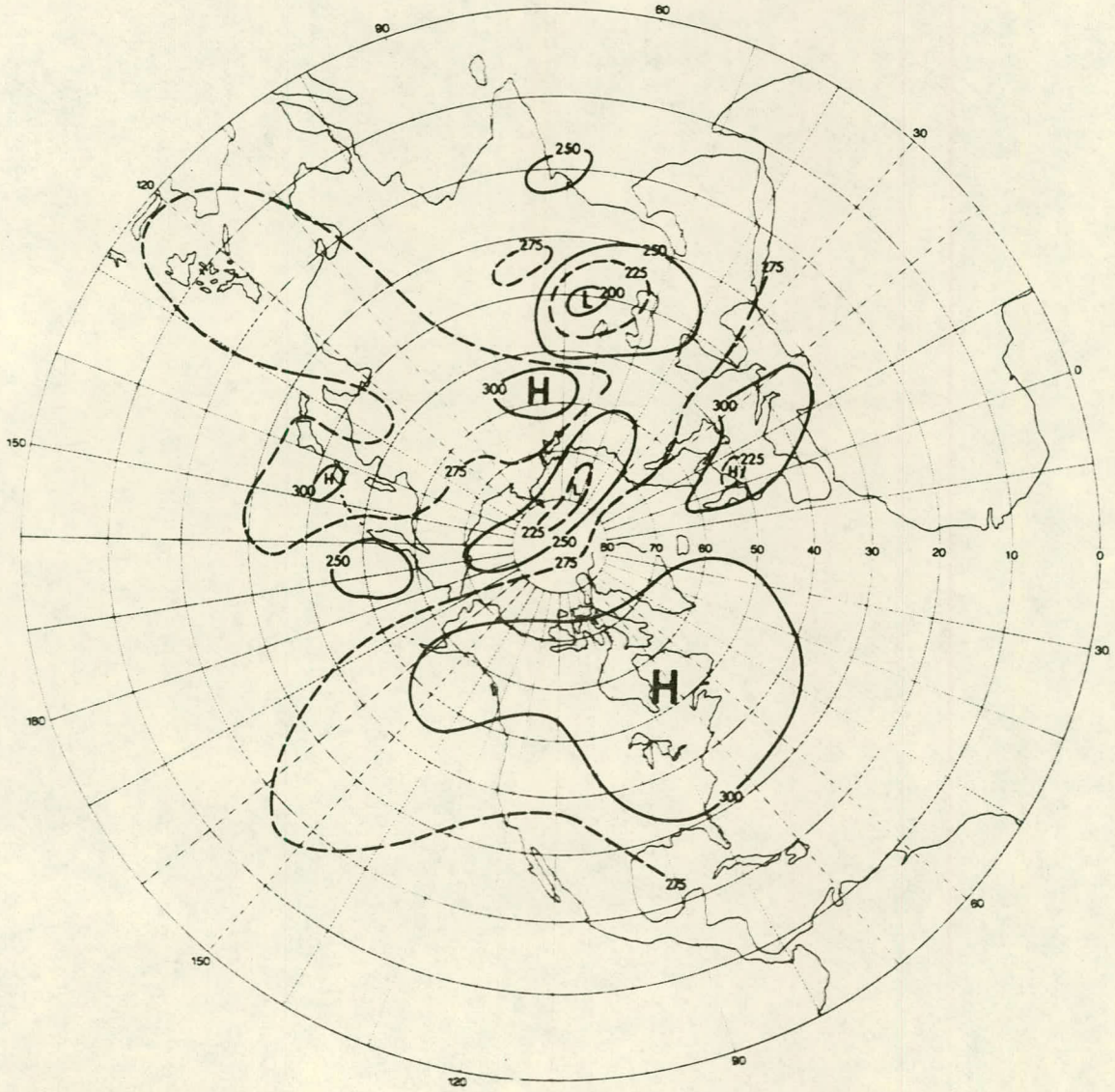

Fig. 24c.

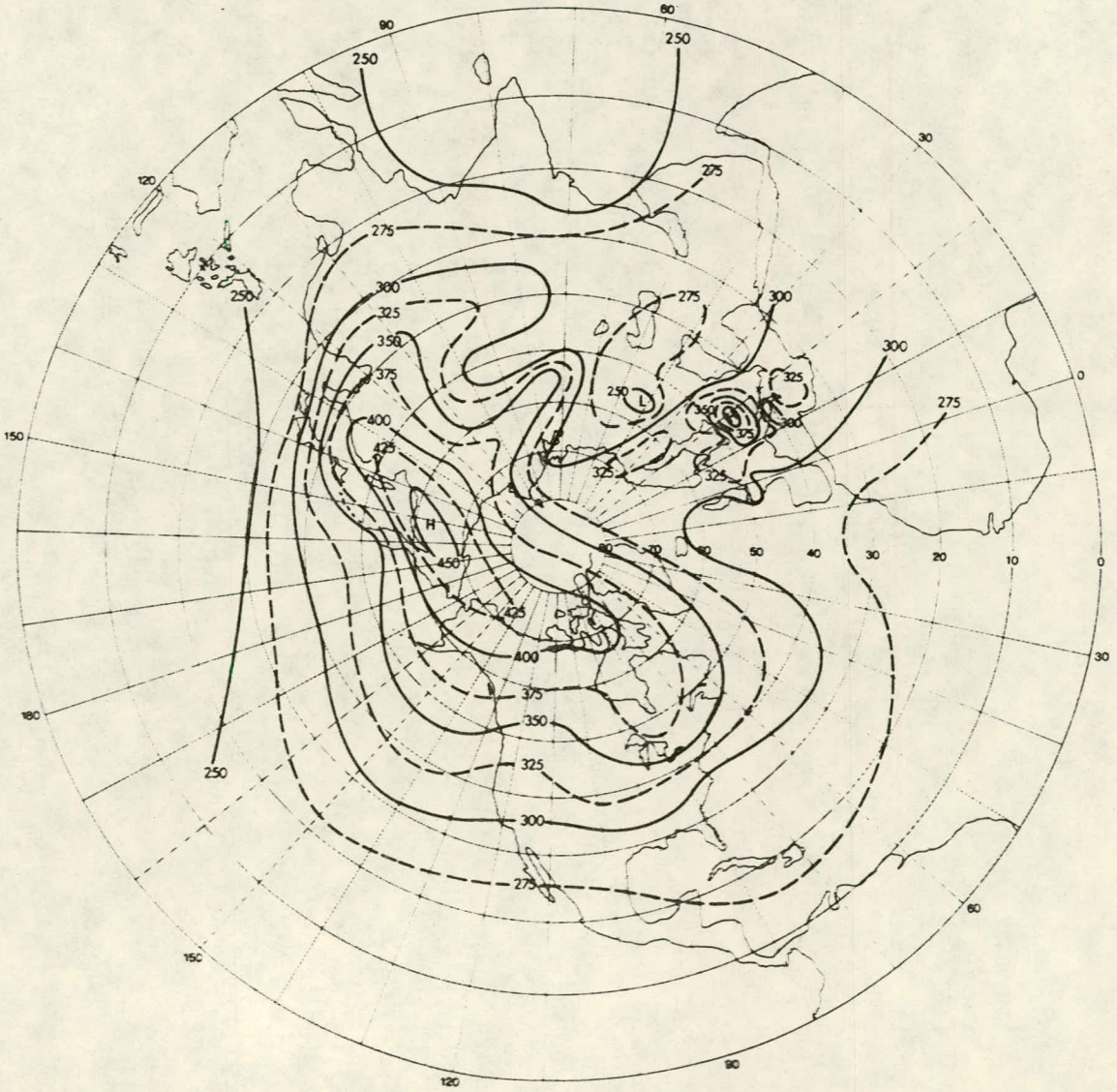

Fig. 24d.

STANDARD DEVIATIONS OF COLUMNAR OZONE

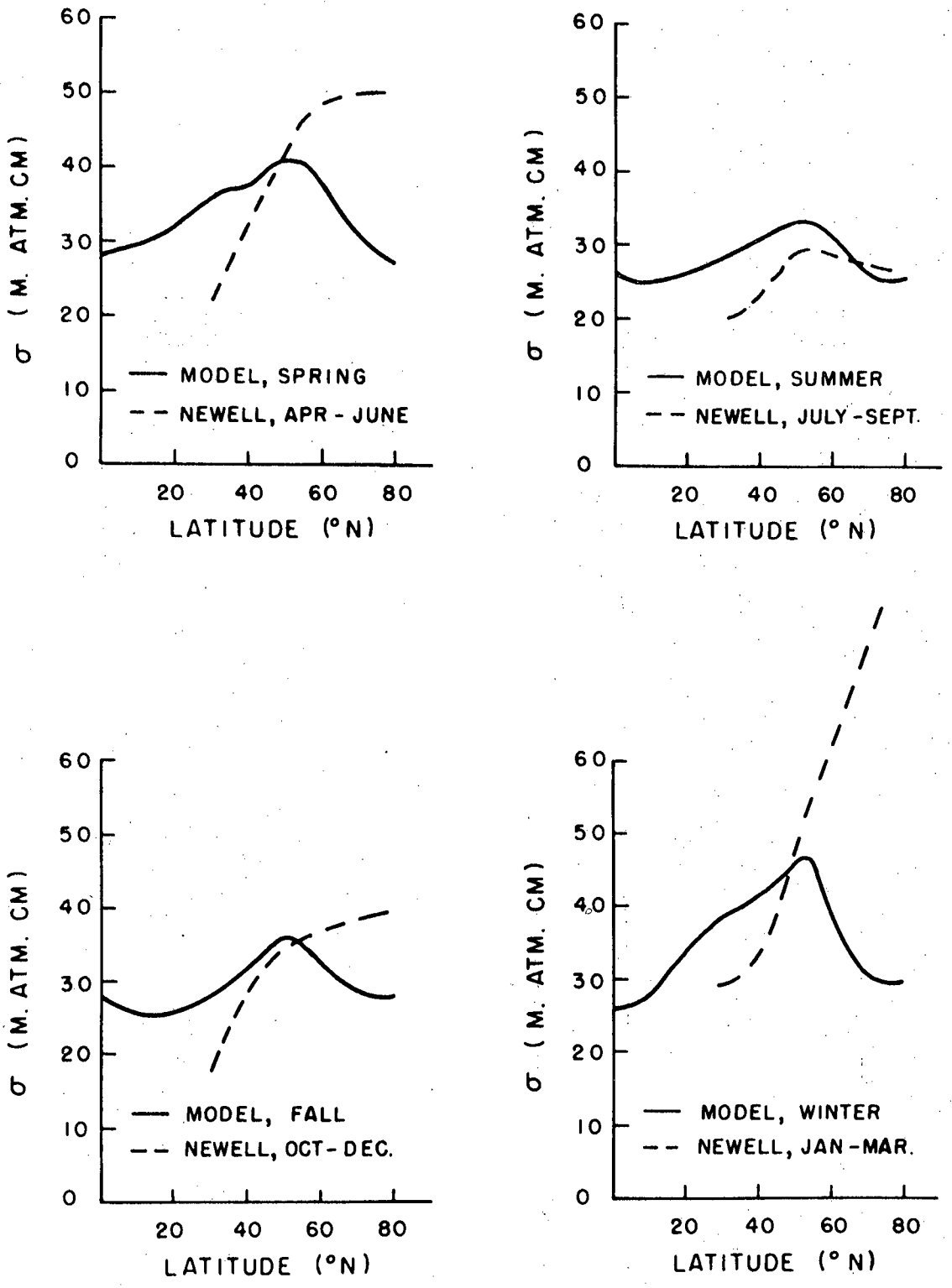

Fig. 25.

Heating of the stratosphere by SST aerosols

by

H. L. Malchow

Draper Laboratory
75 Cambridge Parkway
Mail stop 23
Cambridge, Mass. 02142

I. Introduction

An estimate can be made of the diurnal net heating or cooling of the stratosphere due to the presence of aerosols by using simple calculations that are probably accurate to within a factor of two. The results establish the scale of the aerosol heating and indicate its importance relative to the gases in the heating process. The calculations do not show net effects of the aerosols on the entire vertical heating and radiative transfer structure, but only the net heating at a specific altitude of the gas surrounding an aerosol.

Two types of aerosols are considered, namely the "natural" type of particle consisting largely of sulfuric acid which is potentially formed from SST SO_2 emissions, and SST soot.

The effects of three radiation sources are combined to produce a net radiative heat input to the surrounding gas. Heating is derived from the direct solar flux with a diffuse radiation correction and from surface emission through the 8-12μ window. Cooling is assumed to take place by radiation to space by aerosols at the temperature of the surrounding gases.

II. Heating by Sulfate Aerosols.

Direct Solar Heating This contribution is calculated by evaluations of the integral $\int T(\lambda)F(\lambda)k(\lambda)d\lambda$ where $T(\lambda)$ is the atmospheric transmission from the top of the atmosphere down to the aerosol altitude, $F(\lambda)$ is the solar spectral flux and $k(\lambda)$ is the aerosol absorption cross-section. In the visible wavelength region $T(\lambda)$ and $F(\lambda)$ were obtained from several sources compiled by Malchow (1971). Inthe infra-red $T(\lambda)$ was obtained from the computer code LOWTRAN (Selby 1972). The aerosol absorption cross-section $k(\lambda)$ was computed by a Mie code (K. Cunningham, 1966) using index of refraction (1.5, 0.01i) in the visible wavelength range and (1.4, 0.1i) in the infra-red. Both values are based on the data of Volz (1972). The size distribution used in the Mie code was

$$n(r) = 200\, r^3 e^{-10r^2}.$$

This distribution integrates to unity, peaks near 0.37μ, and has a dispersion of approximately 0.3μ. This distribution agrees with distributions obtained from observations by Mossop (1965) and Bigg (1970).

The wavelength integral has been evaluated numerically over a one day cycle at midlatitude and yields

$$\text{visible, direct heat} = 1.4 \times 10^{-3} \text{ erg/sec/particle}$$

for the visible wavelengths. A diffuse correction factor was obtained by Monte Carlo simulation using the FLASH code (Collins, 1970). At 5500Å and 18 km the diffuse radiation contributes 0.67 times the direct solar flux to the total incident flux. This correction increases the visible light heating to 2.3×10^{-3} erg/sec/particle.

There is also an infra-red contribution to the direct solar heating. The visible light spectral range considered was 0.25 to 0.9μ. Beyond 0.9μ there remains 0.32 of the solar flux. The effective transmission from the top of the atmosphere down to 10 km in the wavelength range 0.9 - 28.μ is approximately 0.99. The average absorption cross-section in this interval is 3.0×10^{-10} cm^2/particle. Then the infra-red direct peak heating rate is 1.4×10^{-4} erg/particle/sec.

When averaged over one day these values are reduced to

visible direct heating = 0.92×10^{-3} erg/sec/particle,

infra-red direct heating = 0.53×10^{-4} "

Cooling to Space

Kirchoffs law can be used to obtain the infra-red energy emission rate from the particles. In general,

$$j_\nu = 4\pi B_\nu k_\nu$$

where j_ν is the total emission coefficient into 4π steradians, k_ν is the absorption corss-section, and B_ν is the Plank function. Over the band width of interest this equation can be averaged over frequency with small error (approximately 6% in this case).

Thus

$$\bar{j} = \frac{\int j_\nu d\nu}{\int d\nu} = \frac{4\pi \int B_\nu k_\nu d\nu}{\int d\nu} \simeq 4\, \bar{B} \cdot \bar{k}.$$

The integrated value of B_ν is $\sigma T^4/\pi$, therefore

$$\bar{j} = 4\sigma T^4 \bar{k}.$$

Let us consider only the upward radiation as true cooling since there will be a radiative exchange between the atmosphere and particle in the lower atmosphere where the optical depths are large. Thus the cooling is reduced to

$$\bar{j} = 2\sigma T^4 \bar{k} \qquad \text{(Eq. 1)}$$

In the stratosphere at 18 km a representative temperature is 220°K. The aerosol temperature is maintained at this value by collisions (See Appendix 1). Over the wavelength range 8μ to 36μ the infra-red value of $\bar{k}$ is approximately $\bar{k} = 2.7 \times 10^{-10}$ cm^2/particle assuming an index of refraction of (1.4, 0.1i).

Upon substituting $\bar{k}$ and T in Eq. 1 one obtains the cooling rate

$$\bar{j} \text{ (infra-red cooling to space)} = 0.69 \times 10^{-4} \text{ erg/sec/particle}$$

at 18 km altitude. Above 18 km the atmospheric transmission in the infra-red is quite high, averaging about 0.9 for the 8μ to 36μ range, therefore this rate is applicable at a range of altitude above 18 km.

Heating by Surface Emission

Heating due to surface emission through the 8 - 12μ window is given by

$$\text{heating (surface)} = \sigma T^4 \bar{k} f \bar{T} \qquad \text{(Eq. 2)}$$

where f is the fraction of black body radiation in the 8 - 12 μ window emitted by the surface, and T is the atmospheric transmission in the window. The mean absorption cross-section in the 8 - 12μ range is 4.7×10^{-10} cm^2/particle, the black body radiation fraction is 0.262, and average transmission is approximately 0.5. If the surface temperature is chosen as 300°K the heating of the particle (surrounding gas) due to the infra-red radiation emitted by the ground is

$$h \text{ (surface)} = 0.29 \times 10^{-4} \text{ erg/sec/particle.}$$

The flux from the surface computed in this way compares very well ($\pm$ 10%) with values obtained by Kuhn and Stearns (1972) via measurements.

Net Heating

Net heating and the contributions of the sources are tabulated below.

Heating		Cooling	
Sun (Vis.)	9.2×10^{-4}	To Space	0.69×10^{-4}
Sun (I.R.)	0.53×10^{-4}		
Surface (300°)	0.29×10^{-4}		
totals	10.0×10^{-4}	-	0.69×10^{-4} → $+ 9.3 \times 10^{-4}$ erg/sec/particle

The heating table shows that the dominant effect is the heating by direct solar flux in the visible wavelength range. If the complex part of the index of refraction in this region is zero as some have suggested (Neumann 1972), then the net heat input at 18 km due to natural aerosols is nearly zero. The results would show (for $n' = 0$) a small net heating of about 10^{-5} erg/sec/particle. However when it is cloudy and the aerosols do not see a 300° K radiating surface there could be a small net cooling of the same order. In units of deg/day these heating and cooling rates would be 0.6×10^{-3} deg/day. The heating rate for $n' = 0.01$ in the visible range is

$$\text{heating } (n' = .01,\ 0.25<\lambda<.9) = 0.057 \text{ deg/day}/(1 \text{ particle/cm}^3)$$

If there were two such particles /cm^3, their contribution to the stratosphere heating at 18 km would be roughly the same as the gaseous contri-

butions. Two particles/cm^3 is consistent with estimates of the current natural background and the SST SO_4 related aerosols (Hidy, 1973). Figure 1 shows the net heating per day at 18 km as a function of the absorption index in the visible light range. At 18 km the aerosol heating effects would be maximized in the sense that their contribution relative to the gaseous heating would be maximized. At higher altitudes the gaseous heating becomes proportionately much larger, and at lower altitudes the aerosols dissipate their heat contribution into a greater gas density thus causing a smaller temperature change.

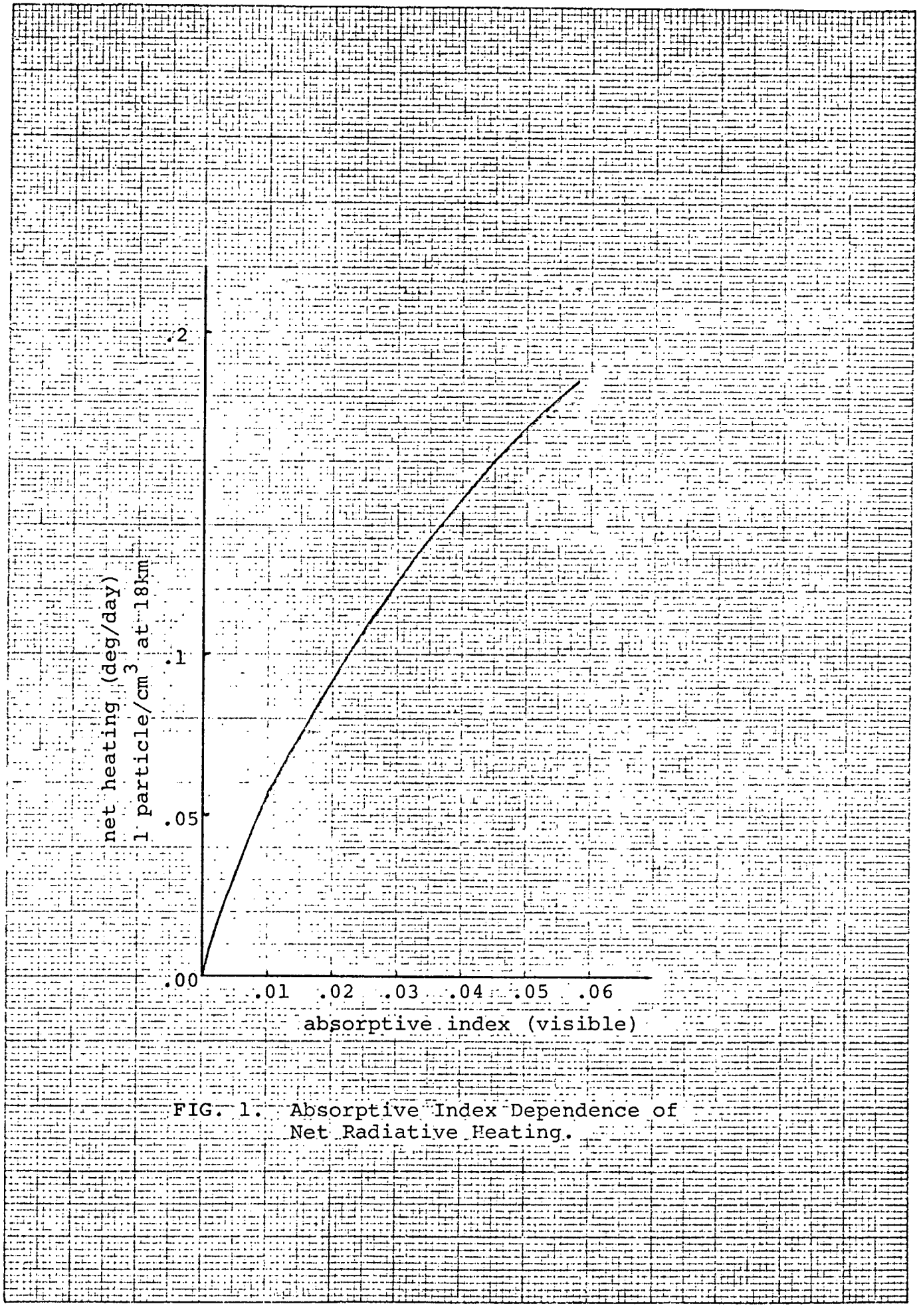

FIG. 1. Absorptive Index Dependence of Net Radiative Heating.

III. Heating by SST Soot

Direct Solar Heating Several filters containing particles deposited by the J-93 engine during the tests at Arnold were analyzed to determine the particle absorption characteristics. Under high altitude cruise conditions most of the filter deposition (~80%) consisted of soot. The absorption of this soot in the infra-red was similar to that of Norit carbon. In the visible wavelength range the material is essentially black and the particles can be assumed to have an absorption cross-section that is approximately equal to their geometric cross-section.

The first measurements of the sizes of these particles by Broderick (1972) indicate radii on the order of 0.1μ. For particles of this size the absorption cross-section is therefore 3.14×10^{-10} cm^2. The direct-plus-diffuse visible light heat production, averaged over one day, is

$$\text{visible, direct heat} = 2.0 \times 10^{-4} \text{ erg/sec/particle.}$$

This is a factor of four smaller than the direct visible solar heating of the sulfate particles having an absorptive index of 0.01. The reduction is due to the smaller dimensions of the soot particles.

Cooling to Space

Applying Kirchoff's law in the form of Eq. 2 one obtains

$$\text{infra-red cooling to space} = 1.2 \times 10^{-5} \text{ erg/particle/sec.}$$

This number is based upon a mean infra-red absorption cross-section of $J_R = 0.43 \times 10^{-10}$ cm^2 which results from an index of refraction (3, 0.5i). The latter value is taken from Volz (1972).

Net Heating by Soot Particles

Since the expected range of soot emissions for SST aircraft has been defined, and the flight loading estimated, one can use these numbers to predict the heating due to soot. Appendix 2 details the relevant number arguements.

The net heating on a per-particle basis is obtained by combining the source numbers listed above.

direct solar	2.0×10^{-4} erg/sec/particle
surface emission	$.27 \times 10^{-5}$
total heating	$\sim 2.0 \times 10^{-4}$ erg/sec/particle
- cooling	$.12 \times 10^{-4}$
net heating	1.9×10^{-4} erg/sec/particle

This heating rate per particle can be multiplied by the particle densities of Appendix 2 to produce the expected heating. The results are summarized as follows:

Region	Heating (Range depending on soot limits)
General Stratosphere	$6.9 \times 10^{-8} \rightarrow 6.9 \times 10^{-6}$ erg/sec
North Atlantic	$0.28 \times 10^{-6} \rightarrow 0.28 \times 10^{-4}$ erg/sec
Far Wake	$1.5 \times 10^{-5} \rightarrow 1.5 \times 10^{-3}$ erg/sec

At 15 km altitude these values lead to the following heating rates in °K/day

Region	Heating (Deg/day)
General Stratosphere	$1.6 \times 10^{-6} \rightarrow 1.6 \times 10^{-4}$
North Atlantic	$0.67 \times 10^{-5} \rightarrow 0.67 \times 10^{-3}$
Far Wake	$0.35 \times 10^{-3} \rightarrow 0.35 \times 10^{-1}$.

IV. Conclusions

Heating by the absorption of direct, visible radiation is the dominant term in the net aerosol heating calculation. This causes a net heating of stratospheric gases in the 15 km region by both sulfate and soot-like aerosols. The heating depends primarily on the value of the complex index of refraction and the particle concentration. For sulfate particles the absorptive index is known to be small, but has not been established with any degree of certainty. Assuming a representative value of 0.01 for this index, the SST sulfate aerosol heating at 15 km is approximately 0.05°K/day. This level of heating is much smaller than the gaseous heating, and is furthermore based upon the pessimistic assumptions that all the SST fuel sulfur will end up as sulfate aerosols, and that the jet fuel will have a moderately high sulfur content. Heating by the soot particles can probably be more accurately assessed at this time. However, because of the relatively small numbers of these particles their heating contribution will be even smaller than the sulfate particle heating. The calculations predict maximum heating levels of roughly 10^{-3}°K/day for the North Atlantic region.

References

Malchow, H.L., (1971) "Standard Models of Atmospheric Constituents and Radiative Phenomena for Inversion Simulation", Internal Report AER-7-1, C.S. Draper Laboratory.

Selby, J.E.A., and McClatchey, R.M., (1972) "Atmospheric Transmittance From 0.25 to 28.5 μm: Computer Code LOWTRAN 2", AFCRL-72-0745.

Cunningham, K., (1966), "Light Transport in the Atmosphere Vol. II: Machine Codes for Calculation of Aerosol Scattering and Absorption Coefficients", AD-650-108.

Volz, F.E., (1972), "The Complex Index of Refraction of Aerosol From 0.2 to 40 μm" in Conference on Atmospheric Radiation, AMS, Fort Collins, Colo., Aug. 7, 1972. pp 114.

Mossop, S.C., (1965), "Stratospheric Particles at 20 km Altitude", Geochimica et Cosmochimica Acta, vol. 29, pp 201.

Bigg, E.K. et al, (1970), "Aerosols at Altitudes Between 20 and 37 km", Tellus, vol. 22, No. 5, pp 550.

Collins, D.G., and Wells, M.B. (1970), "Flash, A Monte Carlo Procedure for use in Calculating Light Scattering in a Spherical Shell Atmosphere", AFCRL-70-0206.

Kuhn, P.M., and Stearns, L.P. (1972), "Radiative Calculation Models for Infra-red Transfer through Cloud, Aerosol and the Continuum", in Conference on Atmospheric Radiation, AMS, Fort Collins, Colo., Aug. 7, 1972. pp 35.

Neumann, J., (1971), "Radiation Absorption by Droplets of Sulfuric Acid Water Solutions and by Ammonium Sulfate Particles", the Hebrew University of Jerusalem Department of Atmospheric Science Contribution No. 72-s.

Broderick, A.J., et al, (1972), "Particles in Jet Aircraft Exhaust: Instrumentation and Final Results", Presented at the 65th Annual Meeting of the Institute of Chemical Engineers, Nov. 1972.

Hidy, G., (1973), in "The Perturbed Stratosphere, 1990", CIAP Vol. 3, Chapter 6.

Appendix 1 : Radiative-Mechanical Heat Transport

Assume spherical particles, that there is a rapid transport of heat within the particle compared to the surrounding air transport, and that the aerosol boundary temperature equals the temperature of the adjacent gas (i.e. equilibrium). Let the mean temperature of the gas be T_o, and the mass density of gas be much larger than the aerosol density. The temperature at the aerosol surface is then given by

$$T = T_o + Q/4\pi rk,$$

where Q is the heating rate, r is the aerosol radius and k is the thermal conductivity. This equation results from the theory developed by Ingersoll[1] who considers a constant "point" heat source in an infinite medium. With constant heat flow at equilibrium, the temperature drop with increasing radius is determined by the thermal conductivity. For a solar constant 1/30 calorie/cm^{2}sec, the maximum possible temperature resulting from aerosol heating is

$$T = T_o + \frac{1/30 \cdot r^2}{4\pi rk} = T_o + \frac{1}{120}\frac{r}{k}$$

where r is particle radius in cm, and $k = 0.055 \times 10^{-3}$ at S.T.P. Assuming k to be proportional to density

$$T = T_o + 1.15 \times 10^5 \frac{r(cm)}{p(mb)}.$$

Values of $T - T_o$ are plotted in the attached figure, and are only seen

---

(1) Heat Conduction, University of Wisconsin Press, Madison, 1954.

Aerosol Equilibrium Temperature Difference. Maximum Value.

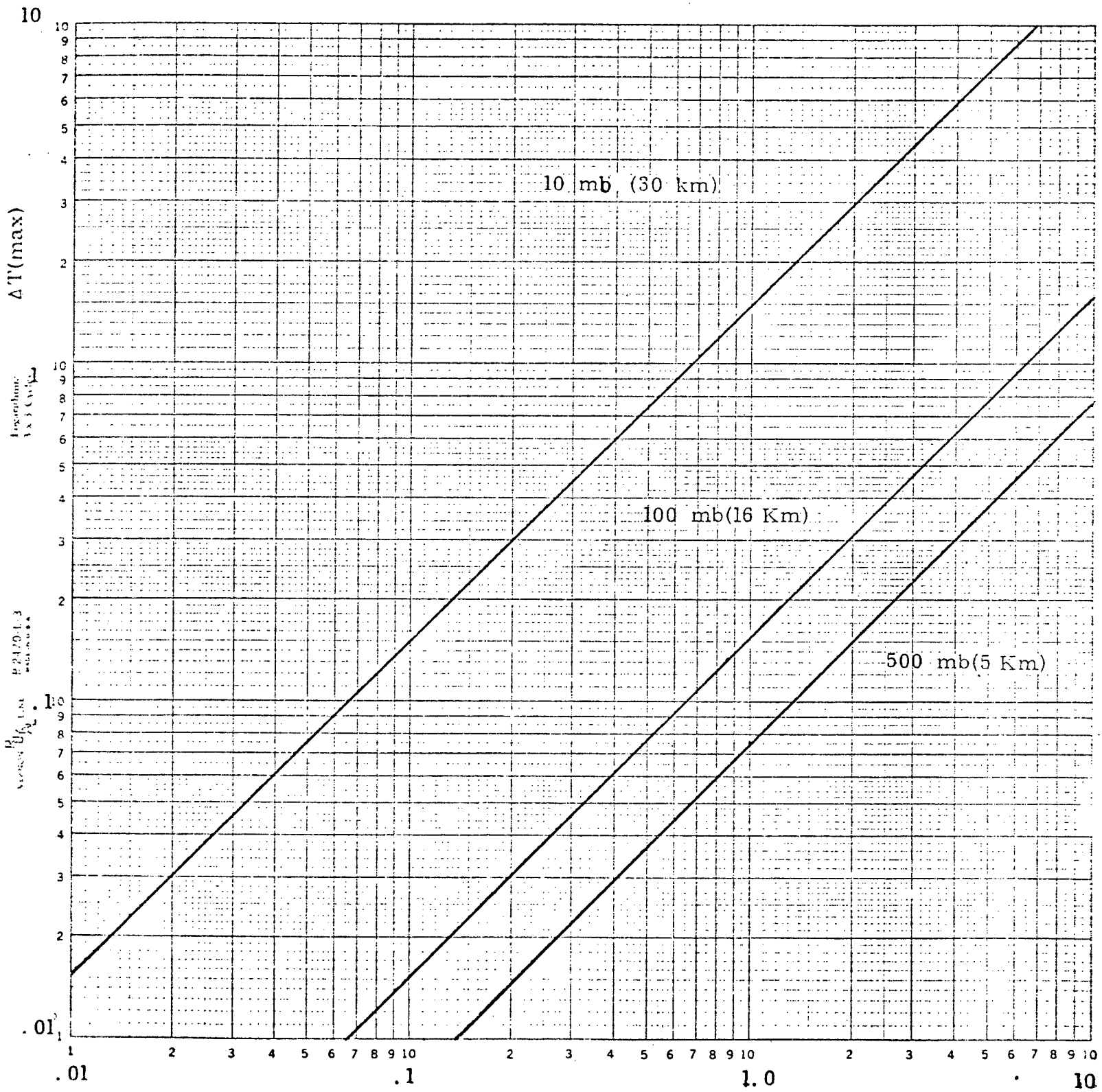

to be significant at high altitudes for large particles.

The above considerations are based upon macroscopic conduction theory and still admit the question: is the collision rate high enough to carry off the accumulated heat?

The collision rate is given by

$$J = \frac{P}{\sqrt{2\pi mkt}} = 0.5 \times 10^{22} \text{ collisions/cm}^2\text{sec}$$

if T = 200°K and P = 10 mb. For a particle of radius 0.1 cm, the collision rate is 0.6×10^{13}/sec. If the energy dissipation rate is 4×10^{-4} ergs/sec, each collision must transfer

$$6.6 \times 10^{-17} \text{ ergs/collision.}$$

However the mean gas molecule energy under these conditions is

$$\frac{1}{2} m\bar{v^2} = \frac{1}{\sqrt{\pi}} \left(\frac{2kT}{1}\right) \Gamma\left(\frac{5}{2}\right) \simeq 4 \times 10^{-14} \text{ergs}$$

and thus the added energy at each collision is approximately 1/1000th of the molecular energy. It would therefore appear that aerosols remain at the temperature of the ambient gas.

Appendix 2 : Basic Numbers relating to Soot Density.

Mass Deposition Rate

The number of SST flights is projected to be about 1700 flights/week[1]. Suppose each flight represents 2 hrs. in the stratosphere, i.e. 3400 flight hours in the stratosphere per week. The particulate fraction, (called emission index when units are gm/kg) is not well determined. Numbers range from[2,3,4,5] 10^{-6} to 10^{-4}. Fuel consumption at cruise is about 50,000 lbs./hr.[2] These numbers yield mass deposition rates in the stratosphere of 170 to 17,000 lbs. of particles per week..

Particle Deposition Rate

Now assume that the particles are all 0.1 μm in radius and of density 1 gm/cm^3. Individual particle volume is $\simeq 4r^3$ or 4×10^{-15} cm^3 and the particle mass is 4×10^{-15} gm. The particle mass in grams is 7.7×10^4 to 7.7×10^6, and the number of particles of 0.1 μm radius is

$$\text{No.} = \frac{\text{particulate mass}}{\text{particle mass}} = 1.93 \times 10^{19} \text{ to } 10^{21} \text{ particles/wk.}$$

This is the number of 0.1 radius particles deposited in the stratosphere per week.

---

(1) R.W. Rummel, pp 34 in Proceedings of the Survey Conference, CIAP, Feb. 15, 1972. DOT-TSC-OST-72-13.

(2) J. Grobman, ibid., pp 25.

(3) T. Broderick, TSC, private communication.

(4) SCEP Report.

(5) Report of an informal meeting held at DOT, Wash. D.C., 6 Oct. 1972, C.E. Junge on Stratospheric Aeroslos.

Stratospheric Volume/Density

The volume of a 1 km. thick layer in the stratosphere is

$$\text{vol.} = 4\pi r^2 \simeq 12\ (6400)^2\ .\ 1\ \text{km}^3$$

or in cm^3, vol. = $4.9 \times 10^{23} \text{cm}^3$.

The particle density in a layer 3 Km thick would then be

$$N/\text{cm}^3 = \frac{\text{Number of Particles}}{\text{Volume of Stratosphere}}$$

$$= \frac{1.93 \times 10^{19} \text{ to } 10^{21} \text{ particles}}{14.7 \times 10^{23}\ \text{cm}^3}$$

$$= 1.31 \times 10^{-5} \text{ to } 10^{-3} \text{ particles/cm}^3\text{/wk}$$

Residence Time

A particle of 0.1 radius with a density of 1 gm/cm^3 has a fall velocity at 16 Km of 1.5×10^{-3} cm/sec. Thus it falls 1 Km in 820 days. So the residence time for particles of this size is long. However, coagulation takes place at a rate which is unknown, and the real residence time is smaller. Some estimates are seven months.(6) (7)

Number Density - Stratosphere

If number densities built up for seven months the density globally would increase to

$$3.6 \times 10^{-4} \text{ to } 3.6 \times 10^{-2} \text{ particles/cm}^3.$$

---

(6) J. Blamount, "Proceedings of the Second Conference on the Climatic Impact Assessment Program", DOT-TSC-OST-73-4, Nov. 1972.

(7) D.J. Hofmann, et al, ibid., pp 23.

Number Density - North Atlantic

In the North Atlantic there are about 350 flights/day, or 700 hours of flight[1] in a volume of roughly $.8 \times 10^{23}$ cm^3. 700 hours of flight produces

$$\frac{700}{3400} \times 2 \times 10^{19 \text{ or } 21} = .41 \times 10^{19 \text{ or } 21} \text{ particles/day}$$

giving a density of $.51 \times 10^{-4}$ to $.51 \times 10^{-2}$ particles/cm^3 per day. Whether this concentration is important or not depends upon the local residence time. If it is a month then there could be 0.15 particles/cm^3 in the North Atlantic region.

Wake Density

In the jet wake the densities are considerably higher. Wake terminal volume is on the order of 100 meters,[8] and the SST cruise speed is roughly 2400 Km/hr. Thus in one hour of flight there is a wake volume of

$$(2.4 \times 10^3 \text{ Km}) \left(10^5 \frac{\text{cm}}{\text{Km}}\right) \cdot (\pi \cdot 10^8 \text{ cm}^2) = 7.55 \times 10^{16} \text{ cm}^3,$$

or $0.6 \times 10^{16-18}$ particles. Thus the far wake density is .08 to 8 particles/cm^3. The larger number is high enough to cause some wake warming and appreciable coagulation over the residence time.

---

(8) T.J. Overcamp, Dispersion of the Exhaust of a Supersonic Transport in the Stratosphere, MIT Ph.D. thesis, Sept. 1972.